Hypoxic tumors are sensitive to FLASH radiotherapy

Ron J Leavitt[1], Aymeric Almeida[1], Veljko Grilj[2], Pierre Montay-Gruel[1, 3, 4], Céline Godfroid[1], Benoit Petit[1], Claude Bailat[2], Charles L Limoli[5], Marie-Catherine Vozenin[1].

[1]Radiation Oncology Laboratory, Department of Radiation Oncology. Lausanne, University Hospital and University of Lausanne, Switzerland

[2] Institute of Radiation Physics, University Hospital and University of Lausanne, Switzerland

[3] Radiation Oncology department, Iridium Netwerk, Wilrijk (Antwerp), Belgium

[4]Antwerp Research in Radiation Oncology (AReRO), Centre for Oncological Research (CORE), University of Antwerp, Belgium

[5] Department of Radiation Oncology, University of California at Irvine, Irvine, CA 92697, USA

Key words: FLASH-RT, hypoxia, radioresistance, metabolic shift.

Funding information: SNFS grant MAGIC- FNS CRS II5_186369. RL and VG (partially) were supported by MAGIC- FNS CRS II5_186369. AA and VG (partially) were supported by NIH grant P01CA244091-01. PMG was supported by FNS N°31003A_156892.

Conflict of Interest Declaration: Authors declare no conflict of interest.

Institutional Animal Care and Use Committee (IACUC) or Other Approval Declaration: The study was approved by the Animal Ethics Council of the Canton of Vaud, Switzerland (number: VD 3241 – VD 3603 – VD 3670).

Acknowledgments: The authors thank Prs J Bourhis and F Bochud for their support, Dr T Boehlen for help in formatting figures, J Ollivier for technical help, K Sprengers for help in radiation experiments. We also thank the Lausanne Genomic Technologies Facility and the animal facility at Epalinges.

Abstract- 144 words (150 max)

Tumor hypoxia is a major cause of resistance to cancer treatments and especially to radiotherapy. To address this specifically, we investigated whether ultra-high dose rate FLASH radiotherapy could overcome this resistance. Tumor cells from various origins were engrafted subcutaneously in mice to provide a reliable and rigorous way to modulate oxygen supply by vascular clamping or carbogen breathing. Tumors were irradiated using a single 20 Gy fraction at both conventional (CONV) and FLASH dose-rates using the Oriatron/eRT6 (PMB-Alcen, FR). Interestingly, and unlike radiotherapy at conventional dose rate, FLASH maintains its anti-tumor efficacy under extreme hypoxia. These findings demonstrate that in addition to normal tissue sparing, FLASH overcomes hypoxia-mediated tumor resistance. Follow-up molecular analysis using RNA-seq profiling uncovered specific metabolic shifts that discriminated FLASH from conventional dose rate irradiation, data that provides specific insights into the mechanism of action and identifies new targets for interventions.

Introduction

In the field of oncology, resistance to treatment is one major cause of therapeutic failure and is often restricted by normal tissue complications. Therefore, overcoming treatment resistance is critical in efforts to enhance the therapeutic index. Resistance to anti-cancer therapies has been investigated intensively and is described as multi-faceted and complex mechanisms that include tumor burden and growth kinetics, tumor heterogeneity, immune suppression, changes in the tumor microenvironment, "undruggable" genomic targets, physical barriers (i.e. blood brain barrier), and hypoxia (reviewed in (1)).

Tumor hypoxia is a primary factor of resistance to radiotherapy (RT), chemotherapy (CT), and immunotherapy (IT). Reduced oxygen tension is very common in solid tumors (2–4), as it develops in response to poor, uneven, and malformed vasculature resulting in acute (proximal to host blood vessel) or chronic (distal to any vasculature) hypoxia. While the lack of oxygen itself is the primary cause of radioresistance, the dysfunctional vasculature is mainly responsible for CT and IT resistance preventing drug access to the tumor. At the cellular level, hypoxia causes rapid activation of hypoxia-inducible factor (HIF) transcription factors (5) as acute survival mechanisms. HIFs transactivate an array of genes involved in angiogenesis, pH balance, cell apoptosis, and a shift to anaerobic metabolism essential for tumor survival and resistance to treatment. Multiple attempts to overcome tumor hypoxia to facilitate effective treatment have been proposed including hypoxia-activated prodrugs, hyperbaric oxygen breathing, 60% supplemental oxygen, allosteric hemoglobin modifiers, molecules that improve oxygen diffusion, and oxygen transport agents (hemoglobin-based or fluorocarbon-based) (6). Most of these strategies have led to negative results and enhanced normal tissue toxicity. To date, no effective anti-cancer therapies against hypoxic tumors is available.

Previously, our team developed a novel radiotherapy approach called FLASH-RT that utilizes ultra-high-dose-rate (UHDR) irradiation beams (7–13). The main interest of FLASH-RT is its capacity to enhance the therapeutic window of radiotherapy by sparing normal tissue from radiation-induced toxicities while eliciting the same tumor kill when compared to iso-doses of conventional dose-rate RT, a biological effect that has been called the FLASH effect. While certain technological limitations are the main obstacle for the clinical translation of FLASH-RT (RV Vozenin et al, NRCO). understanding the differential impact that FLASH-RT has at the normal tissue *versus* tumor level remains an important goal to further understand the mechanisms of the FLASH effect (RV Limoli et al, ARCB). Classical radiobiological dogma posits that radiolytic depletion of oxygen induced by irradiation at UHDR would cause a transient protective hypoxia in the healthy tissue, while hypoxic tumors would be minimally affected (14). This hypothesis has now been challenged by experimental measurements, where radiolysis-induced hypoxia after UHDR in normal tissues and tumors was found to be minimal (< 0.2%) after exposure to therapeutic doses (2-10 Gy) (15). In another hypothesis, FLASH-RT has been proposed to protect stem cells known to be preferentially located in hypoxic niches (16). However, this also suggests that hypoxic tumors and cancer stem cells would be protected, contrary to the dose-rate independence of tumor cell kill. Clearly, further in-depth investigations are warranted before embarking on clinical transfer.

In light of the foregoing, it is noteworthy that nearly every preclinical cancer model tested has shown identical tumor growth delay (TGD) when FLASH-RT and conventional-dose-rate RT (CONV-RT) are compared (7,15,17–20). However, these studies mainly consisted of small volume tumors, and to date, no investigations evaluating FLASH-RT have been performed on extremely hypoxic, radio-resistant tumors. To rectify this critical gap in knowledge, we focused the present study to address the impact of varying tumor oxygenation on FLASH-RT. Here we implemented a validated a model of subcutaneous tumors that provides a reliable and rigorous way modulate oxygen supply by vascular

clamping or carbogen breathing. Unlike CONV-RT, we highlight here that FLASH-RT maintains its anti-tumor efficacy ***even under extreme hypoxia***. Subsequent molecular analysis using RNA-seq profiling was performed at acute and relapse time points, and data pointed toward specific metabolic shifts following FLASH- versus CONV-RT, which inform on the mechanism of action.

Results

Severe induced hypoxia under vascular clamping protects tumors from CONV-RT but not FLASH-RT in various murine subcutaneous tumor models

We sought to determine the impact of oxygen tension on tumor control using FLASH-RT. To this end, we used a human glioblastoma (GBM; U-87 MG) xenograft model implanted subcutaneously in the flask of female Swiss Nude (immunodeficient) mice. We modulated the tumor oxygen tension using a vascular clamp (hypoxia) and carbogen breathing (hyperoxia). Tumor oxygen tension was measured via real-time oxygen readings using the Oxyphor PtG4 probe (Oxygen Enterprises Ltd., **Figure 1B**) and hypoxia was confirmed post-treatment using pimonidazole staining (**Figure S4**). The TGD results are shown in **Figure 1A**. For CONV-RT-treated tumors (left panel), TGD correlated directly with the intra-tumoral oxygen tension; with lower oxygen tension (clamp condition) leading to less tumor control, and higher oxygen tension (carbogen breathing) leading to more effective tumor control compared to the physioxia condition. FLASH- and CONV-RT were similar in delaying the growth of physoxic and hyperoxic tumors. Conversely, FLASH-RT was more effective to delay the growth of hypoxic tumors compared to CONV-RT, and no statistical difference was found between hypoxic and physoxic tumor growth after FLASH-RT. This result has been replicated several times in the same model (**Figure S1**) and confirmed with H454 mouse GBM grafted in the same mouse strain (**Figure S2**). Additionally, SV2 mouse lung cancer and MEERL95 mouse head-and-neck cancer were grafted in both Swiss nude mice and immunocompetent C57BL6/J mice and achieved similar results – see **Figures S3-S4**. Our data indicates that FLASH-RT is a promising approach for the treatment of hypoxic tumors.

Evidence of a tumor relapse profile and FLASH-RT-specific metabolic changes at the late timepoint

To determine the mechanism of FLASH-RT anti-tumor efficacy under hypoxic conditions, we performed bulk RNA-seq at early (24 hours post-RT) and late (one-week post-tumor-recurrence) timepoints. A general data overview for both timepoints is presented in **Figure 2**. Overall more top-level transcriptional differences are observed in the 24-hour timepoint (**Figure 2A**, principle component (PC) 1 accounting for 78% of variance) compared to the late timepoint (**Figure 2B**, PC1 accounting for 39% of variance). For the samples taken at the late timepoint post-RT, principle components analysis (PCA; **Figure 2B**) revealed that the non-irradiated controls cluster together well (circle, left), but all of the RT-treated tumors clustered without distinction based on RT modality or oxygenation condition. This suggests that this late-time point imprint is more related to relapse than to radiation response. The 24-hour heatmap (**Figure 2C**) indicates FLASH-RT samples (green) tended to be further removed from the main cluster of NIR samples (blue) than CONV-RT (red), with few exceptions. The late timepoint heatmap (**Figure 2D**) supports the assertion that NIR (blue) samples cluster well together (center). This is also reflected in the PCA (**Figure 3A**) and heatmap (**Figure 3B**) of the top 500 genes excluding the hyperoxia condition, where unsupervised clustering shows that the non-irradiated samples group together and show similar profiles (**Figure 3A** left and **Figure 3B** center-left). The RT treatment groups are not particularly cohesive or homogenous, indicating lots of intra-group sample-to-sample variability. Due to the lack of cohesive group clustering, overrepresentation analysis (ORA) could not

be performed using well-segregated heatmap clusters or lists of genes above a certain log2 fold change cutoff or below an adjusted p-value cutoff. However, it was still possible to look for signatures of gene sets based on the total set of differentially expressed genes between groups using gene set enrichment analysis (GSEA) and looking for FLASH-specific enrichments (gene sets changed significantly *versus* non-irradiated control in both FLASH physioxia and FLASH hypoxia groups, but not in neither of the CONV-RT groups). Interestingly, this analysis revealed that upregulation of metabolic gene sets (mitochondrial genes, mitochondrial translation, and oxidative phosphorylation (OXPHOS)), inflammation-related gene sets (COVID-19, acute inflammatory response, non-alcoholic fatty liver disease), and the amino acid metabolism gene set were specific to FLASH-RT treated samples at this late timepoint (**Figure 3C**).

GSEA comparison analysis reveals FLASH-specific and tumor delay outcome signatures in GBM tumor response at acute timepoint

RNA-seq results from the early timepoint samples are shown in **Figure 4A-B,** using PCA and a dendrogram heatmap to visualize sample-to-sample distances and clustering. With the same strategy as the one used for overlap analysis, FLASH-specific and tumor delay outcome (changed significantly versus non-irradiated control for FLASH hypoxia, FLASH physioxia, and CONV physioxia groups, but not the CONV hypoxia group) enrichments were investigated. We also included gene sets that were altered significantly for all IR groups versus NIR for reference. For the WikiPathways database (**Figure 4C-D**), it appeared as though downregulation of OXPHOS and electron transport chain and concordant upregulation of glycolysis/gluconeogenesis are associated with the tumor delay outcome and not FLASH-specific. For the FLASH-specific enrichments, notable upregulated sets were: NRF2 pathway, focal adhesion, and complement and coagulation cascades. The FLASH-specific downregulated sets included pathways of ribosomal proteins, transcription, and purine metabolism.

Overlaps in GSEA of specific transcription factor and miRNA binding sites were then investigated (Molecular Signatures Database C3: Regulatory Target Gene Sets; **Figure 4, E-F**). Increased expression of NFκB and HIF1 signaling targets appeared to be associated with the tumor delay outcome. In the FLASH-RT-specific group, an increase in expression of miR-149-3p targets was observed, whereas it was not modified in the CONV hypoxia vs. non-irradiated comparison. In terms of sets with expression decreases – the "FOXR2_TARGET_GENES" and "ZNF704_TARGET_GENES" were the only gene sets found for the TGD overlap. For the FLASH-specific overlap of downregulated sets – the "RORA_target_genes" set was the most significant and there was only one miRNA in the top 10 (shown), which was miR-372-5p. Collectively these GSEA overlap profiles provide a clearer picture about the transcriptional landscape in RT-treated *versus* native tumors at 24 hours post-RT, and which changes are FLASH-RT-specific.

ORA analysis of FLASH-upregulated and FLASH-downregulated clusters at 24 hours for hypoxic condition

As the significant difference in TGD between FLASH-RT and CONV-RT was observed in the hypoxic condition, we examined the expression data in this particular group more closely. PCA (**Figure 5A**) of 24-hour samples irradiated under hypoxia conditions showed that expression levels in the FLASH-RT-treated samples were the most distant from the untreated tumor samples. This is particularly the case in PC1 – which accounted for 79% of the total variance in the analysis. Unsupervised hierarchical clustering of the top 500 genes displayed in a heatmap format (**Figure 5B**) reinforces this observation,

as the biological groups cluster together very well with the non-irradiated group (blue) clustering closer to the CONV-RT group (red) than the FLASH-RT group (green). Furthermore, the genes segregate neatly into two clusters (left): genes that are up in FLASH (Cluster 2, light green) and genes that are down in FLASH (Cluster 1, gray).

Using the two clusters of genes, we performed ORA for terms that were enriched from the WikiPathways (**Figure 5, C and E**) and Gene Ontology (Biological Processes Only, **Figure 5, D and F**) databases among others. Cluster 1 genes (down in FLASH) enriched terms involved ribosomes, translation, mRNA catabolism, OXPHOS, and mitochondria, whereas Cluster 2 genes (up in FLASH) enriched terms included glycolysis, gluconeogenesis, HIF-1 signaling, hypoxia response, focal adhesion and purine metabolism.

GSEA and pathway analysis highlight significant differences in cell cycle signaling, hypoxia/HIF-1a signaling, p53 signaling, and cell metabolism between FLASH-RT-treated and CONV-RT-treated tumors at 24 hours post-RT under hypoxic condition

To further characterize differences in gene expression of hypoxic tumors 24h after irradiation with FLASH and CONV-RT, GSEA was performed using the hallmark gene sets database (**Figure 6A)**. Cell cycling gene sets (Hallmark E2F Targets and Hallmark G2M Checkpoint) were downregulated (normalized enrichment score (NES) = -2.87, adjusted p-value = 3.13×10^{-25} and NES = -2.52, adjusted p-value = 9.74×10^{-16}, respectively) after FLASH, while the Hallmark p53 Pathway (NES = 1.46, adjusted p-value = 0.0172) and Hallmark Apoptosis (NES = 1.46, adjusted p-value = 0.0235) gene sets were upregulated. Overall, under the hypoxia condition, hypoxia (NES = 2.77, adjusted p-value = 2.96×10^{-23}) and glycolysis (NES = 1.87, adjusted p-value = 8.56×10^{-6}) pathways gene expression was increased in FLASH, while oxidative phosphorylation (NES = -2.25, adjusted p-value = 1.24×10^{-10}) gene expression was decreased.

Examination of the hypoxia and metabolic pathways (**Figures 6, B-D**), showed numerous upregulated targets downstream HIF1A (red, **Figure 6B**) – including targets related to anaerobic metabolism. Specifically, we observed an upregulation of PDK-1, which, in turn, causes inhibition of the TCA cycle and electron transport chain and stimulation of glycolysis. Therefore, the upregulation of the main glycolytic pathway was consistent (red, **Figure 6C**) in the FLASH-RT treated tumors compared to the CONV-RT treated tumors under hypoxia. At the same time, the section of the pathway where pyruvate is converted into acetyl-CoA for the TCA cycle was downregulated (blue), which is consistent with a lack of aerobic respiration. In fact, it appears possible that the oxaloacetate intermediate was being shunted back into the glycolytic/gluconeogenic pathway. Further reinforcing the ORA and GSEA data, the KEGG oxidative phosphorylation pathway (**Figure 6D**) was downregulated in FLASH-RT versus CONV-RT samples across all five electron transport chain (ETC) complexes. Each complex I-V has multiple components downregulated consistent with significant ETC repression/disruption. The unsupervised clustering of all the metabolic genes from these two pathways using a heatmap (**Figure 6E**) with all conditions from the 24-hour timepoint showed that the genes separated into two clusters: one including mostly OXPHOS genes and one composed including mostly glycolysis/gluconeogenesis genes. The FLASH-RT treated samples from all oxygen conditions clustered mostly together with the OXPHOS cluster downregulated and the glycolysis cluster upregulated. In contrast, the CONV-RT treated samples clustered mostly with the non-irradiated ones with higher expression in the OXPHOS cluster and lower expression in the glycolysis one. These data highlight clear differences in tumor metabolism at 24 hours post-RT when treated with 20 Gy FLASH versus CONV electrons, which could be causing the observed difference in tumor control under hypoxic conditions.

Discussion

The key finding of this study demonstrates that FLASH-RT is as effective against severely hypoxic tumors as it is for physoxic tumors. This result was not restricted to a single model but was reproduced and validated in multiple different human and murine tumor models implanted in immunodeficient and immunocompetent mouse strains. RNA-seq analysis of bulk tumor samples at acute (24-hour) and late (one week post-relapse) timepoints provided mechanistic insight to the anti-tumor efficacy triggered by FLASH-RT in hypoxic tumors as well as possible targets for combined treatments.

Tumor hypoxia represents one of the major root causes of cancer treatment resistance, and thus hypoxic tumors are extremely difficult to treat using CONV-RT, chemotherapies, and even immunotherapies. The relationship between tumor oxygenation and the efficacy of radiotherapy at conventional dose rate is well-known and has been extensively characterized (4). This relationship is directly reflected in our present data, where more oxygenated tumors benefit from a greater growth delay, whereas less oxygenated tumors are more poorly controlled. Nevertheless, the results obtained in our study using FLASH-RT reverses this paradigm completely. For rigor, tumor oxygenation was measured directly and non-invasively, where severe hypoxia (1-2 mmHg O_2, < 0.5% O_2) was confirmed within minutes after clamping (15,21–24). The same methodology confirmed that carbogen breathing resulted in a modest increase in tumor pO_2 consistent with the literature (25,26). However, with the Oxyphor 2P system we measure average oxygen in the tumor to roughly 2-3 mm in depth, but is not optimized to visualize heterogeneous oxygen normalization in previously non-oxygenated area. This highly hypoxic fraction of the tumors dominate the regrowth of the tumor since they are more radioresistant and there a small increase of oxygen could lead to significant radiosensitization. Our results also suggest that the sensitivity of tumors to FLASH-RT is not restricted to a single and/or specific model but can be generalized, as results were replicated in various human GBM (U-87 MG), murine GBM (H454), head-and-neck cancer (mEERL95) and lung adenocarcinoma (SV2) models and in both immunocompromised and competent hosts, thereby dismissing a specific contribution of the adaptive immune system.

To address the implicit mechanistic question and since a simple nodular tumor model was used, bulk tumor transcriptome sequencing was performed at acute and late timepoints post-RT under all the same conditions that were used in the TGD studies. Interestingly, expression changes observed at acute timepoint were no longer observed at late timepoint (one week after recurrence). These late-timepoint expression profiles were relatively similar in all samples (with PC1 and PC2 both less than 35%), and even more so in the irradiated groups, suggesting tumor-recurrence-driven changes more than radiation-induced changes. The different oxygenation and radiation modality conditions did not result in differential-expression-based clustering. Nonetheless, differences were noted in the expression profiles induced by RT versus NIR controls. In particular, OXPHOS/mitochondrial gene sets are significantly upregulated in FLASH-RT-treated tumors (with both oxygenation conditions) seven days post-recurrence. These results correlate with studies present in the literature showing a higher treatment resistance in OXYPHOS-dependent, dormant, and slow-cycling tumor stem cells (27–29). However, these gene sets being enriched to a greater extent in FLASH- versus CONV-RT treated tumors may indicate that FLASH-RT causes stronger metabolic selection.

At the early timepoint (24 hours post-RT), multiple cell cycle genes and pathways were found altered, corresponding to a well described response to RT (30). These gene sets – most notably cell cycle, DNA replication, and E2F transcription factor targets – were significantly downregulated to the NIR controls in all IR conditions, regardless of oxygenation condition. From this, we inferred that these pathway

alterations were unlikely to cause the difference seen in TGD post-FLASH-RT under hypoxia. A significant downregulation of DNA repair, IR-induced DNA damage response, and ATM/ATR activation was observed for all IR conditions versus the NIR control group. It is likely that 24 hours may be too late for detecting this rapid response to single- and double-stranded DNA breaks and this profile could only catch the aftermath of the rapid activation of these pathways within minutes and hours post-RT.

Thus, moving forward with the analysis we sought to find significant (adjusted p-value < 0.05) gene set enrichments that were specific to FLASH-RT treatment and ones were more broadly associated with effective tumor control. Starting with the FLASH-specific enrichments, the NRF2 pathway was a significantly upregulated gene set. As the master regulator of the antioxidant response, NRF2 (*NFE2L2*) is described to be activated in response to cellular oxidative stress (31). This finding suggests that the profile detected at acute time point identified mainly pro-survival genes and pathways. In addition, it was also unexpected as FLASH-RT was showed to induce less total H_2O_2 generation compared to CONV-RT in simple (water) systems (11). Alternatively, this result might suggest that FLASH-RT directly activates the NRF2 pathway, pointing to key differences in the redox homeostasis between tumors vs. healthy tissue after FLASH-RT exposure. Further, reactive oxygen species (ROS) balance, buffering capacity, and labile iron pools could be the major dividers between healthy and cancerous cells (32). A significant downregulation of cytoplasmic ribosomal proteins was also observed specifically in the FLASH-RT groups. This was detected both in the FLASH-specific GSEA and by the cluster 1 ORA enrichments, with biological processes such as cytoplasmic translation, translation initiation, ribosome biogenesis, protein targeting to ER, and protein folding all being significantly downregulated in the FLASH-RT treated samples. Given the large energy toll of mRNA translation into protein (33), downregulation of ribosomal machinery for all but essential functions, stress response, and DNA repair is consistent with enhanced cell survival, but if tumors cannot compensate to meet the needs of macromolecular synthesis, they succumb to FLASH-RT just as after CONV-RT. Indeed, transient, radiation-induced inhibition of cap-dependent protein synthesis is a conserved cellular stress response (34). Much of the immediate response (within hours) is controlled at the translation initiation level, but evidence of transcript-level changes were found here at 24 hours post-RT. In summary, these results show that FLASH-RT enhances cellular stress at the tumor level and thus effects a stronger stress response, likely promoting isoeffective tumor cell kill.

Further analysis, showed that the TGD outcome was associated with significant metabolic alterations at 24 hours post-RT, specifically decreased OXPHOS and increased glycolysis gene expression. These changes are consistent with recently described changes in cellular metabolism in cancer cell lines following IR *in vitro* (35), but these expression changes were either not significant or even changed in the opposite direction (OXPHOS upregulated, though not significantly) when comparing the CONV hypoxia group to the non-irradiated tumor group. Therefore, we concluded that FLASH-RT modulates expression of these metabolic gene sets under severe hypoxia, while CONV-RT does not. These metabolic changes were further highlighted and reinforced by ORA cluster analysis, GSEA, pathway analysis, and heatmap clustering of metabolic genes and were most likely enacted by the hypoxia-inducible factor 1 (HIF-1) transcription factor. Under hypoxic conditions, HIF1A protein dimerizes with HIF1B and the resulting active HIF-1 complex translocates to the nucleus where it binds to hypoxia response elements (HREs) and directs transcription of numerous hypoxia response genes. These genes include metabolic regulators (*PGK1*, *HK2*, *PDK1*), promoters of angiogenesis (*VEGFA*), glucose transporters (*GLUT1*), and vascular tone modulators (*eNOS*, *HMOX1*). On the contrary, under physoxic conditions, HIF1A is hydroxylated, ubiquitinated and degraded by the proteasome before it can form HIF-1 complexes and access the nucleus (36). HIF-1 has been shown to be activated in many cancers, including GBM (37), facilitating aerobic glycolysis in cancer cells, as originally described by Otto Warburg ((38); known as Warburg Effect). In this study, we found that HIF-1 targets are being

upregulated significantly compared to the native tumor levels 24 hours after FLASH-RT and not after CONV-RT when irradiated under severe hypoxia.

HIF-1 activation following RT is described in the literature, including a dose-dependent increase in HIF-1 activity post-RT starting at 12 hours and reaching a peak at about 2 days in 4T1 tumors *in vivo* (39). This phenomenon was described as a result of the reoxygenation-induced ROS influx and depolymerization of stress granules containing sequestered HIF-1 target transcripts. Reoxygenation occurs post-RT due to a combination of reperfusion and decrease in oxygen consumption of irradiated tumor cells (40). This feature of decreased oxygen consumption in irradiated tumor tissue is consistent with our data showing decreased OXPHOS gene expression post-RT. ROS have been shown to be both necessary and sufficient for HIF-1 activation and evidence of ROS presence was observed in FLASH-RT-treated tumors. Paradoxically, both HIF-1 and NRF2 signaling are generally considered as potent cellular pro-survival genes. HIF-1 has specifically been shown to direct the synthesis of protective cytokines for endothelial cells (39), and is considered to be a key factor in radioresistance. However, in our results, the upregulation of HIF-1 targets is associated with more effective tumor control outcomes. These strong survival programs are activated in response to cellular stress. We hypothesize that FLASH-RT cause significantly more cellular stress in tumors under hypoxia than CONV-RT. Designing treatments that take advantage of the downstream metabolic shift resulting from the FLASH-RT-specific HIF-1 activation in hypoxic tumors could be of major importance.

The "FLASH effect" has now been validated to elicit normal tissue sparing while retaining equivalent tumor control at isoeffective dose compared to CONV-RT. Interestingly, results show that the former aspect is insensitive to decreased oxygen tension whereas the latter is sensitive to increased oxygen tension (11). Moreover, activation of a FLASH-specific stress response was identified and was shown as significantly and positively correlated with tumor response outcome. To our knowledge, this is the first study showing that FLASH-RT retains anti-tumor efficacy under hypoxia. This major finding provides significant insight into the mechanism of action of the FLASH effect. Thus, in conjunction with normal tissue sparing efficacy, FLASH-RT could solve hypoxia-mediated radiation resistance, as most solid tumors treated by radiotherapy are hypoxic. This bodes well for clinical translation once larger tumors can be effectively targeted with this innovative irradiation modality.

Materials and Methods

Animal experiments

158 Female Swiss Nude mice (NU(Ico)-*Foxn1*^{nu}) were purchased from CRL France. Female C57BL6/J mice (Charles River) and C57BL/6JRJ (Janvier Labs) were purchased for subcutaneous tumor experiments using SV2 lung adenocarcinoma and mEERL95 Head&Neck tumor models, respectively. Animal experiments were approved by Swiss Ethics Committee for Animal Experimentation (VD 3241 – VD 3603 – VD 3670) and performed within institutional guidelines.

Irradiation devices

Irradiation was performed using a prototype 6 MeV electron beam linear accelerator (LINAC) of type Oriatron 6e (eRT6; PMB Alcen), available at Lausanne University Hospital and described previously (41). Physical dosimetry has been extensively described and published to ensure reproducible and reliable biological studies. This LINAC is able to produce a pulsed electron beam at a mean dose rate ranging from 0.1 Gy·s−1 (i.e., comparable to conventional dose rates used in RT) up to 5.106 Gy·s−1,

corresponding to a dose, in each electron pulse, ranging from 0.01 up to 10 Gy. All FLASH irradiations were performed at a mean dose rate above 100 Gy/s and at a dose rate within the pulse above $1.8.10^6$ Gy/s. The beam parameters used throughout this study are included in Table 1. The irradiation settings corresponding to the prescription dose for mouse irradiations were determined by surface dose measurements on a 30 × 30 cm^2-solid water slab positioned behind a 1.7 cm-diameter aperture of a graphite applicator (13.0 × 13.0 × 2.5 cm^3), as previously described.

Tumor model *in vivo* irradiations and follow-up

The U-87 MG subcutaneous human glioblastoma model consists of injecting 10 million U-87 MG human GBM cells (ATCC) contained in 100 µl 1xPBS in the right flank of female Swiss Nude mice. 1 million SV2 lung adenocarcinoma cells contained in 100µl (40% matrigel Matrix (356234, Corning), 60% 1xPBS) were implanted in the flank of C57BL6/J mice. 500 000 mEERL95 Head&Neck tumor cells were resuspended in 100 µl 1xPBS and injected in the flank of C57BL/6JRJ mice. The tumor volume was measured thrice weekly with the aid of caliper and calculated using the formula for an oblate ellipsoid (width^2 x length/2). Irradiations were performed when tumor volume reached a mean between 60 - 80 mm^3. Mice were randomly separated in two different irradiation groups (FLASH or CONV-RT) and three different oxic-conditions groups (hypoxia, physioxia, hyperoxia). Mean tumor volumes were similar in all groups (n= 5-6 animals per group).

All irradiations of subcutaneous tumor bearing mice were performed under isoflurane anesthesia. Tumors were irradiated by positioning the tumor-bearing part of the skin in extension behind and in contact with the opening of the 1.7 cm diameter graphite applicator, while limiting the dose to the intestines. A 5 mm solid water plate was placed behind the skin to ensure homogenous dose delivery. For irradiations under hyperoxic conditions, mice were anesthetized with isoflurane and carbogen (95% O_2, 5% CO_2) for at least 20 min, including the irradiation time. For irradiations in hypoxic conditions, tumors were clamped with a vascular clamp at least 15 min before and during the irradiation. All tumors were treated with a single dose of 20 Gy. For all regimen, FLASH and CONV irradiation modalities were compared. Mice were sacrificed when tumors reached 750 mm^2 or were showing indications of necrosis.

Oxygen measurements performed with Oxyphor2P Probe and Detectors

On the day of the experiment, the animals were anesthetized in an induction box (3-4% isoflurane) and then with a mask (1-2% isoflurane for maintenance) on a heating mat to maintain the animal's temperature at 37°C. Vitamin A in ophthalmic cream (Vitapos®) was applied to the eyes of the animal to prevent drying. Once anesthetized, 25uL of Oxyphor PtG4 probe (200 µM) was injected intravenously. After 30 minutes to ensure the spread and accumulation of probe, the optical fiber was placed about 1 cm from the tumor to ensure the measurement. All measurements were performed under anesthesia.

Validation of the different oxygen conditions with Pimonidazole

To validate the different oxygenation conditions of the tumors, mice (n=4 for each group) were injected retro-orbitally with Pimonidazole (Hypoxyprobe HP1-100Kit) at 60 mg / kg 90 min before the sampling. For nornoxic conditions, injection was followed by 90 min air breathing. For hyperoxic

conditions, injections was followed by 90 min carbogen breathing. For hypoxic conditions, injection was followed by 15 min air breathing then 7 min tumor clamping and 68 min air breathing.

Tumors were then collected, fixed in FineFix (Biosystems), embedded in paraffin and finally cut into 4 µm sections. Tumors hypoxia were validated on tumor sections using mouse anti-pimonidazole monoclonal antibody (1:50; Hypoxyprobe HP1-100Kit) incubated 1h at room temperature. The sections were then incubated for 1h with a donkey anti-mouse AF488 secondary antibody (1:250; Life Technologies A21202). Image acquisition was performed using an upright Zeiss Axiovision microscope.

RNA extraction

For the RNA-seq study, mice (n=3-6 for each group) were irradiated in the same condition and the same dose of the TGD study. Tumors were sampled 24h after radiotherapy and were disrupted in cold RLT lysis buffer with automated homogenizer (TissueLyser II, Qiagen) and total RNA extracted using the RNEasy mini kit (Qiagen) according to manufacturer instructions. RNA quality (RQN > 6.8) was assessed on a Fragment Analyzer (Agilent Technologies). RNA-seq libraries were prepared from 500 ng of total RNA with the Illumina TruSeq Stranded mRNA reagents (Illumina) using a unique dual indexing strategy, and following the official protocol automated on a Sciclone liquid handling robot (PerkinElmer). Libraries were quantified by a fluorimetric method (QubIT, Life Technologies) and their quality assessed on a Fragment Analyzer (Agilent Technologies).

Cluster generation was performed with 2 nM of an equimolar pool from the resulting libraries using the Illumina HiSeq 3000/4000 SR Cluster Kit reagents and sequenced on the Illumina HiSeq 4000 using HiSeq 3000/4000 SBS Kit reagents for 150 cycles (single end).

RNAseq Analysis

Raw FASTQ files were uploaded to the European Galaxy server (www.usegalaxy.eu) for further manipulation and processing. Read quality was assessed using FastQC. Read trimming was not necessary (42) so we proceeded straight to alignment. The RNA STAR aligner (version 2.7.8a, (43)) was used to align the reads to the human genome (hg38, for the human tumor cells) and the mouse genome (mm10, for the mouse vasculature within the tumor sample), with NM-tag turned on for XenofilteR. Binary alignment (BAM) files from all sequencing lanes for each sample were merged at this point (within alignments to the same species) using the Samtools merge tool (version 1.13, (44)). These merged and paired alignments for each sample were used as input for XenofilteR (version 1.6, (45)) for filtering of mouse reads from the human alignment, which was implemented in R (version 4.1.0, (46)) using the RStudio environment (version 1.4.1717, (47)). These filtered reads were then counted for annotated genes using featureCounts (version 2.0.1, (48)) in Galaxy. Raw counts tables were imported back into RStudio for differential gene expression and pathway analyses using the DESeq2 (version 1.34.0, (49)) and clusterProfiler (version 4.2.0, (50)) packages. Plots were generated using the ggplots2 (version 3.3.5, (51)) and pheatmap (version 1.0.12, (52)) packages.

Statistical analyses

Statistical analyses were carried out using GraphPad Prism (v8) software. P values were derived from t-test adjusted with the Holm-Šidak method. Results were expressed as mean values ± SEM, and all analyses considered a value of $P \leq 0.05$ to be statistically significant unless specified otherwise.

Figure Legends

Figure 1: FLASH-RT, unlike CONV-RT, maintains equivalent tumor control even in severely hypoxic tumors. **(A)** Relative tumor volume of U87 implanted subcutaneously in the flank of female Nude mice treated with 20 Gy single fraction delivered with CONV (**left**) or FLASH (**right**) radiation therapy with different oxygenation conditions (physioxia – hxpoxia – hyperoxia). Mean fold change ± SEM, *N* = 5-18 animals per group. *P* values were derived the Holm-Sidak t test against the FLASH physioxia group: **P* < 0.05; ****P* < 0.001; *****P* < 0.0001; ns, not significant. **(B)** Kaplan–Meier survival curves for patients stratified by radiation modality and tumor oxygenation. **(C)** Representative real-time oxygen measurements from a subcutaneous U87 tumor *in vivo* taken using the OxyPhor 2P (Oxygen Enterprises Ltd.) phosphorescent probe with platinum core injected intravenously and detected using the laser attachment and detector are shown for the three different oxygenation conditions (physioxia, vascular clamp, and carbogen breathing). Signal averaging line is shown in bold.

Figure 2: Data Overview. Principal components analysis (PCA) was performed to visualize sample-to-sample distances based on the top two principal components (PC1 and PC2) for 24-hour **(A)** and late **(B)** timepoints. Non-irradiated control cluster highlighted with a circle at the late timepoint. Heatmaps for both timepoints **(C and D, respectively)** are displayed for the top 500 genes – with columns (samples) and rows (genes, Z-score) were clustered hierarchically.

Figure 3: Comparison overlap analysis of GSEA at late timepoint. **(A)** Principal components analysis (PCA) was performed to visualize sample-to-sample distances based on the top two principal components (PC1 and PC2), specifically for the physioxia and hypoxia conditions. **(B)** A heatmap was generated with the same samples showing the top 500 genes – columns (samples) and rows (genes, Z-score) were clustered hierarchically. **(C)** Gene set enrichment analysis (GSEA) was performed at the late timepoint comparing each treatment group with the non-irradiated (NIR) controls. This heatmap figure displays the FLASH-RT-specific gene set enrichments upregulated at the late timepoint. Numbers shown represent the normalized enrichment scores generated by the GSEA. Only the "FLASH_phys vs. NIR" and "FLASH_hypo vs. NIR" scores were significant (adjusted p-value < 0.05).

Figure 4: Comparison overlap analysis of GSEA at early timepoint. **(A)** Principal components analysis (PCA) was performed to visualize sample-to-sample distances based on the top two principal components (PC1 and PC2), specifically for the physioxia and hypoxia conditions. **(B)** The sample-to-sample distance plot further displays the clustering of the groups, with darker blue indicating greater similarity. Gene set enrichment analysis (GSEA) was performed at the 24-hour timepoint comparing each treatment group with the non-irradiated (NIR) controls. The number of gene sets in each overlap is displayed is displayed in the Venn diagrams for genes upregulated **(C, E)** and downregulated **(D, F)** when interrogating the Wikipathways **(C, D)** and regulatory targets **(E, F)** databases. For each of the overlaps circled in the Venn Diagram, a number of gene sets are shown in the heatmap figure showing the normalized enrichment scores of each comparison. For the "FLASH-specific" gene sets, only the FLASH groups were significantly (adjusted p-value < 0.05) upregulated or downregulated from the NIR control. For the "Tumor Delay Outcome" gene sets, the FLASH physioxia, FLASH hypoxia and CONV physioxia were significantly (adjusted p-value < 0.05)

upregulated or downregulated from the NIR control, while the CONV hypoxia group was not. For the "All IR" gene sets, all groups were significantly (adjusted p-value < 0.05) upregulated or downregulated from the NIR control.

Figure 5: Cluster-based ORA analysis for the 24-hour hypoxia condition. (**A**) Principal components analysis (PCA) was performed to visualize sample-to-sample distances based on the top two principal components (PC1 and PC2). (**B**) A heatmap was generated with the same samples showing the top 500 genes – columns (samples) and rows (genes, Z-score) were clustered hierarchically. Genes were clustered into cluster 1 (mostly down in FLASH-RT) and cluster 2 (mostly up in FLASH-RT). Clusters 1 and 2 were used for overrepresentation analysis (ORA) using both Wikipathways **(C, D)** and gene ontology (GO; **E, F)** databases. Wikipathways enrichments are presented in barcharts and GO enrichments are presented in treeplots.

Figure 6: GSEA enrichments and metabolic pathways for FLASH vs. CONV comparison in the 24-hour hypoxia expression data. **(A)** Gene set enrichment analysis (GSEA) results are shown for selected hallmark gene sets. All results shown are for the comparison FLASH-RT-treated versus CONV-RT-treated tumors sampled at 24 hours post-RT. Normalized enrichment score indicates gene sets upregulated in the FLASH condition (positive numbers) or downregulated in the FLASH condition (negative numbers). GSEA plots of selected gene sets are highlighted. Expression differences are displayed for KEGG pathways: HIF-1 signaling pathway **(B)**, the glycolysis/gluconeogenesis pathway **(C)**, and the oxidative phosphorylation pathway **(D)**, rendered by the Pathview package. Using just the glycolysis/gluconeogenesis and oxidative phosphorylation pathway genes, a heatmap **(E)** was able to cluster hierarchically most of the FLASH-treated samples together by the 24-hour expression values.

Supplemental Figure Legend

Figure S1: Relative tumor volume of U-87 MG human GBM cells implanted in subcutaneous of female Nude mice treated with 20 Gy single fraction delivered with CONV (left) or FLASH (right) radiation therapy with different oxygenation conditions (physioxia – hypoxia – hyperoxia). These were the animals that were sampled for the late timepoint RNA-seq analysis. Mean fold change ± SEM, N = 4-7 animals per group. P values were derived the Holm-Sidak t test against the FLASH physioxia group: **P* < 0.05; ****P* < 0.001; *****P* < 0.0001; ns, not significant.

Figure S2: Relative tumor volume of H454 mouse GBM cells implanted in subcutaneous of female Nude mice treated with 20 Gy single fraction delivered with CONV (left) or FLASH (right) radiation therapy with different oxygenation conditions (physioxia – hypoxia – hyperoxia). Mean fold change ± SEM, N = 6-7 animals per group. P values were derived the Holm-Sidak t test against the FLASH physioxia group: *P < 0.05; **P < 0.01; ****P < 0.0001; ns, not significant.

Figure S3: Relative tumor volume of SV2 mouse lung adenocarcinoma cells implanted in subcutaneous of female Swiss nude (left) or C57Bl6 (right) mice treated with 20 Gy single fraction delivered with CONV or FLASH radiation therapy with different oxygenation conditions (physioxia – hxpoxia). Mean fold change ± SEM, N = 4-6 animals per group. P values were derived the Holm-Sidak t test against the FLASH physioxia group: *P < 0.05; ns, not significant.

Figure S4: Relative tumor volume of MEERL95 mouse head and neck carcinoma cells implanted in subcutaneous of female Swiss nude (left) or C57Bl6 (right) mice treated with 20 Gy single fraction delivered with CONV or FLASH radiation therapy with different oxygenation conditions (physioxia – hxpoxia). Mean fold change ± SEM, N = 6-7 animals per group. P values were derived the Holm-Sidak t test against the FLASH physioxia group: *P < 0.05; ns, not significant.

Figure S5: PIMO immunostaining on tumor sections after manipulating oxygenation conditions: physioxia, vascular clamp, or carbogen breathing without radiotherapy. Green, PIMO; Blue, DAPI.

References

1. Vasan N, Baselga J, Hyman DM. A view on drug resistance in cancer. Nature. 2019;575:299–309.

2. Vaupel P, Höckel M, Mayer A. Detection and Characterization of Tumor Hypoxia Using pO2 Histography. Antioxidants & Redox Signaling. Mary Ann Liebert, Inc., publishers; 2007;9:1221–36.

3. Zhu W, Dong Z, Fu T, Liu J, Chen Q, Li Y, et al. Modulation of Hypoxia in Solid Tumor Microenvironment with MnO2 Nanoparticles to Enhance Photodynamic Therapy. Advanced Functional Materials. 2016;26:5490–8.

4. Moulder JE, Rockwell S. Hypoxic fractions of solid tumors: Experimental techniques, methods of analysis, and a survey of existing data. International Journal of Radiation Oncology*Biology*Physics. 1984;10:695–712.

5. Zeng W, Liu P, Pan W, Singh SR, Wei Y. Hypoxia and hypoxia inducible factors in tumor metabolism. Cancer Letters. 2015;356:263–7.

6. Graham K, Unger E. Overcoming tumor hypoxia as a barrier to radiotherapy, chemotherapy and immunotherapy in cancer treatment. IJN. 2018;Volume 13:6049–58.

7. Favaudon V, Caplier L, Monceau V, Pouzoulet F, Sayarath M, Fouillade C, et al. Ultrahigh dose-rate FLASH irradiation increases the differential response between normal and tumor tissue in mice. Sci Transl Med. 2014;6:245ra93.

8. Montay-Gruel P, Petersson K, Jaccard M, Boivin G, Germond JF, Petit B, et al. Irradiation in a flash: Unique sparing of memory in mice after whole brain irradiation with dose rates above 100Gy/s. Radiother Oncol. 2017;124:365–9.

9. Montay-Gruel P, Bouchet A, Jaccard M, Patin D, Serduc R, Aim W, et al. X-rays can trigger the FLASH effect: Ultra-high dose-rate synchrotron light source prevents normal brain injury after whole brain irradiation in mice. Radiother Oncol. 2018;129:582–8.

10. Vozenin MC, De Fornel P, Petersson K, Favaudon V, Jaccard M, Germond JF, et al. The Advantage of FLASH Radiotherapy Confirmed in Mini-pig and Cat-cancer Patients. Clin Cancer Res. 2019;25:35–42.

11. Montay-Gruel P, Acharya MM, Petersson K, Alikhani L, Yakkala C, Allen BD, et al. Long-term neurocognitive benefits of FLASH radiotherapy driven by reduced reactive oxygen species. Proc Natl Acad Sci U S A. 2019;116:10943–51.

12. Bourhis J, Sozzi WJ, Jorge PG, Gaide O, Bailat C, Duclos F, et al. Treatment of a first patient with FLASH-radiotherapy. Radiotherapy and Oncology. 2019;139:18–22.

13. Alaghband Y, Cheeks SN, Allen BD, Montay-Gruel P, Doan NL, Petit B, et al. Neuroprotection of Radiosensitive Juvenile Mice by Ultra-High Dose Rate FLASH Irradiation. Cancers (Basel). 2020;12.

14. Wilson JD, Hammond EM, Higgins GS, Petersson K. Ultra-High Dose Rate (FLASH) Radiotherapy: Silver Bullet or Fool's Gold? Frontiers in Oncology [Internet]. 2020 [cited 2022 Apr 12];9. Available from: https://www.frontiersin.org/article/10.3389/fonc.2019.01563

15. Cao X, Zhang R, Esipova TV, Allu SR, Ashraf R, Rahman M, et al. Quantification of Oxygen Depletion During FLASH Irradiation In Vitro and In Vivo. International Journal of Radiation Oncology*Biology*Physics. 2021;111:240–8.

16. Pratx G, Kapp DS. Ultra-High-Dose-Rate FLASH Irradiation May Spare Hypoxic Stem Cell Niches in Normal Tissues. International Journal of Radiation Oncology*Biology*Physics. 2019;105:190–2.

17. Fouillade C, Curras-Alonso S, Giuranno L, Quelennec E, Heinrich S, Bonnet-Boissinot S, et al. FLASH Irradiation Spares Lung Progenitor Cells and Limits the Incidence of Radio-induced Senescence. Clinical Cancer Research. 2020;26:1497–506.

18. Chabi S, To THV, Leavitt R, Poglio S, Jorge PG, Jaccard M, et al. Ultra-high-dose-rate FLASH and Conventional-Dose-Rate Irradiation Differentially Affect Human Acute Lymphoblastic Leukemia and Normal Hematopoiesis. International Journal of Radiation Oncology*Biology*Physics. 2021;109:819–29.

19. Ruan J-L, Lee C, Wouters S, Tullis IDC, Verslegers M, Mysara M, et al. Irradiation at Ultra-High (FLASH) Dose Rates Reduces Acute Normal Tissue Toxicity in the Mouse Gastrointestinal System. International Journal of Radiation Oncology*Biology*Physics. 2021;111:1250–61.

20. Montay-Gruel P, Acharya MM, Gonçalves Jorge P, Petit B, Petridis IG, Fuchs P, et al. Hypofractionated FLASH-RT as an Effective Treatment against Glioblastoma that Reduces Neurocognitive Side Effects in Mice. Clinical Cancer Research. 2021;27:775–84.

21. Dunphy I, Vinogradov SA, Wilson DF. Oxyphor R2 and G2: phosphors for measuring oxygen by oxygen-dependent quenching of phosphorescence. Analytical Biochemistry. 2002;310:191–8.

22. Esipova TV, Karagodov A, Miller J, Wilson DF, Busch TM, Vinogradov SA. Two New "Protected" Oxyphors for Biological Oximetry: Properties and Application in Tumor Imaging. Anal Chem. American Chemical Society; 2011;83:8756–65.

23. Esipova TV, Barrett MJP, Erlebach E, Masunov AE, Weber B, Vinogradov SA. Oxyphor 2P: A High-Performance Probe for Deep-Tissue Longitudinal Oxygen Imaging. Cell Metabolism. 2019;29:736-744.e7.

24. El Khatib M, Van Slyke AL, Velalopoulou A, Kim MM, Shoniyozov K, Allu SR, et al. Ultrafast Tracking of Oxygen Dynamics During Proton FLASH. International Journal of Radiation Oncology*Biology*Physics. 2022;113:624–34.

25. Martin L, Lartigau E, Weeger P, Lambin P, Le Ridant AM, Lusinchi A, et al. Changes in the oxygenation of head and neck tumors during carbogen breathing. Radiotherapy and Oncology. 1993;27:123–30.

26. Falk SJ, Ward R, Bleehen NM. The influence of carbogen breathing on tumour tissue oxygenation in man evaluated by computerised p02 histography. Br J Cancer. Nature Publishing Group; 1992;66:919–24.

27. Viale A, Pettazzoni P, Lyssiotis CA, Ying H, Sánchez N, Marchesini M, et al. Oncogene ablation-resistant pancreatic cancer cells depend on mitochondrial function. Nature. Nature Publishing Group; 2014;514:628–32.

28. Lagadinou ED, Sach A, Callahan K, Rossi RM, Neering SJ, Minhajuddin M, et al. BCL-2 Inhibition Targets Oxidative Phosphorylation and Selectively Eradicates Quiescent Human Leukemia Stem Cells. Cell Stem Cell. 2013;12:329–41.

29. Viale A, Corti D, Draetta GF. Tumors and Mitochondrial Respiration: A Neglected Connection. Cancer Research. 2015;75:3687–91.

30. Wang B. Analyzing Cell Cycle Checkpoints in Response to Ionizing Radiation in Mammalian Cells. In: Noguchi E, Gadaleta MC, editors. Cell Cycle Control: Mechanisms and Protocols [Internet]. New York, NY: Springer; 2014 [cited 2022 Aug 22]. page 313–20. Available from: https://doi.org/10.1007/978-1-4939-0888-2_15

31. Vomund S, Schäfer A, Parnham MJ, Brüne B, Von Knethen A. Nrf2, the Master Regulator of Anti-Oxidative Responses. International Journal of Molecular Sciences. Multidisciplinary Digital Publishing Institute; 2017;18:2772.

32. Spitz DR, Buettner GR, Petronek MS, St-Aubin JJ, Flynn RT, Waldron TJ, et al. An integrated physico-chemical approach for explaining the differential impact of FLASH versus conventional dose rate irradiation on cancer and normal tissue responses. Radiotherapy and Oncology. 2019;139:23–7.

33. Li G-W, Burkhardt D, Gross C, Weissman JS. Quantifying Absolute Protein Synthesis Rates Reveals Principles Underlying Allocation of Cellular Resources. Cell. 2014;157:624–35.

34. Braunstein S, Badura ML, Xi Q, Formenti SC, Schneider RJ. Regulation of Protein Synthesis by Ionizing Radiation. Molecular and Cellular Biology. American Society for Microbiology; 2009;29:5645–56.

35. Krysztofiak A, Szymonowicz K, Hlouschek J, Xiang K, Waterkamp C, Larafa S, et al. Metabolism of cancer cells commonly responds to irradiation by a transient early mitochondrial shutdown. iScience. 2021;24:103366.

36. Semenza GL. Signal transduction to hypoxia-inducible factor 1. Biochemical Pharmacology. 2002;64:993–8.

37. Kaynar MY, Sanus GZ, Hnimoglu H, Kacira T, Kemerdere R, Atukeren P, et al. Expression of hypoxia inducible factor-1α in tumors of patients with glioblastoma multiforme and transitional meningioma. Journal of Clinical Neuroscience. 2008;15:1036–42.

38. Warburg O, Wind F, Negelein E. THE METABOLISM OF TUMORS IN THE BODY. Journal of General Physiology. 1927;8:519–30.

39. Moeller BJ, Cao Y, Li CY, Dewhirst MW. Radiation activates HIF-1 to regulate vascular radiosensitivity in tumors: Role of reoxygenation, free radicals, and stress granules. Cancer Cell. 2004;5:429–41.

40. Kallman RF. The Phenomenon of Reoxygenation and Its Implications for Fractionated Radiotherapy. Radiology. Radiological Society of North America; 1972;105:135–42.

41. Jaccard M, Durán MT, Petersson K, Germond J-F, Liger P, Vozenin M-C, et al. High dose-per-pulse electron beam dosimetry: Commissioning of the Oriatron eRT6 prototype linear accelerator for preclinical use. Medical Physics. 2018;45:863–74.

42. Liao Y, Shi W. Read trimming is not required for mapping and quantification of RNA-seq reads at the gene level. NAR Genomics and Bioinformatics. 2020;2:lqaa068.

43. Dobin A, Davis CA, Schlesinger F, Drenkow J, Zaleski C, Jha S, et al. STAR: ultrafast universal RNA-seq aligner. Bioinformatics. 2013;29:15–21.

44. Li H, Handsaker B, Wysoker A, Fennell T, Ruan J, Homer N, et al. The Sequence Alignment/Map format and SAMtools. Bioinformatics. 2009;25:2078–9.

45. Kluin RJC, Kemper K, Kuilman T, de Ruiter JR, Iyer V, Forment JV, et al. XenofilteR: computational deconvolution of mouse and human reads in tumor xenograft sequence data. BMC Bioinformatics. 2018;19:366.

46. R Core Team. R: A Language and Environment for Statistical Computing. R Foundation for Statistical Computing [Internet]. 2021; Available from: https://www.R-project.org/

47. RStudio Team. RStudio: Integrated Development Environment for R. RStudio, PBC [Internet]. 2021; Available from: http://www.rstudio.com/

48. Liao Y, Smyth GK, Shi W. featureCounts: an efficient general purpose program for assigning sequence reads to genomic features. Bioinformatics. 2014;30:923–30.

49. Love MI, Huber W, Anders S. Moderated estimation of fold change and dispersion for RNA-seq data with DESeq2. Genome Biology. 2014;15:550.

50. Wu T, Hu E, Xu S, Chen M, Guo P, Dai Z, et al. clusterProfiler 4.0: A universal enrichment tool for interpreting omics data. The Innovation. 2021;2:100141.

51. Wickham H. ggplot2: Elegant Graphics for Data Analysis [Internet]. Springer-Verlag New York; 2016. Available from: https://ggplot2.tidyverse.org

52. Kolde R. pheatmap: Pretty Heatmaps. R package version 1.0. 12. CRAN R-project org/package= pheatmap. 2019;

Fig. 1

A.

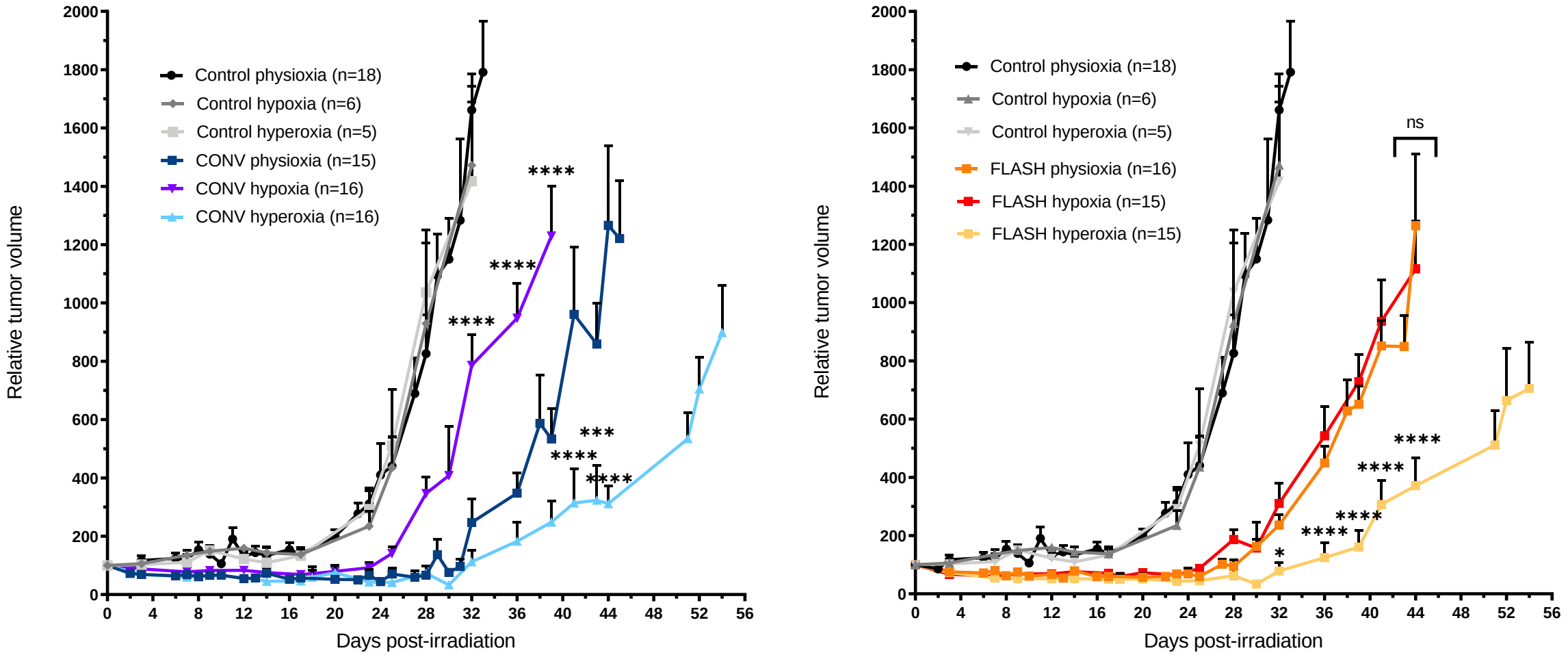
Relative tumor volume
Days post-irradiation
Control physioxia (n=18)
Control hypoxia (n=6)
Control hyperoxia (n=5)
CONV physioxia (n=15)
CONV hypoxia (n=16)
CONV hyperoxia (n=16)
FLASH physioxia (n=16)
FLASH hypoxia (n=15)
FLASH hyperoxia (n=15)
****
***
*
ns

B.

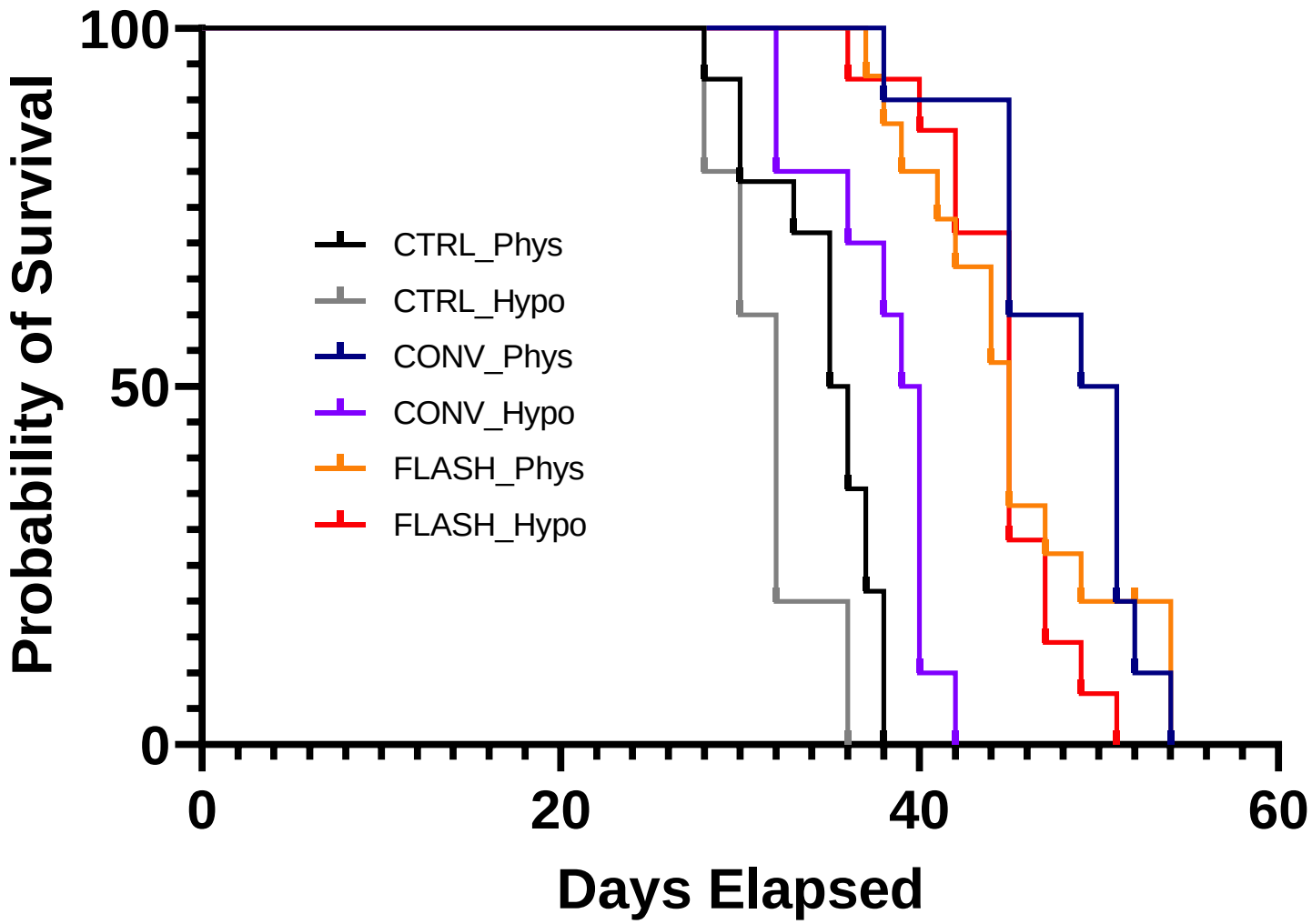
100
50
0
Probability of Survival
0
20
40
60
Days Elapsed
CTRL_Phys
CTRL_Hypo
CONV_Phys
CONV_Hypo
FLASH_Phys
FLASH_Hypo

C.

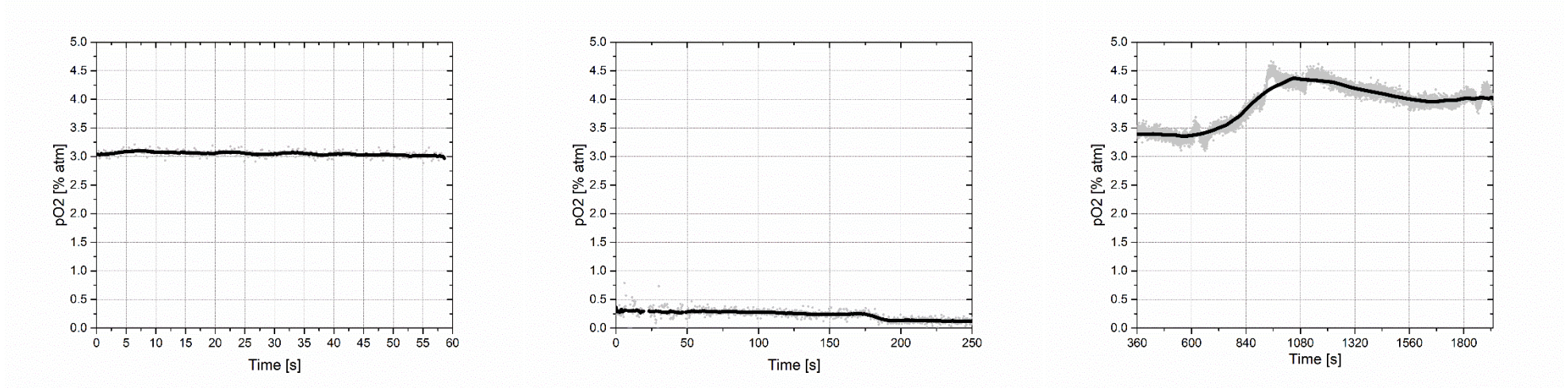

Physioxia

Vascular Clamp

Carbogen Breathing

Figure 2: Data Overview

A.

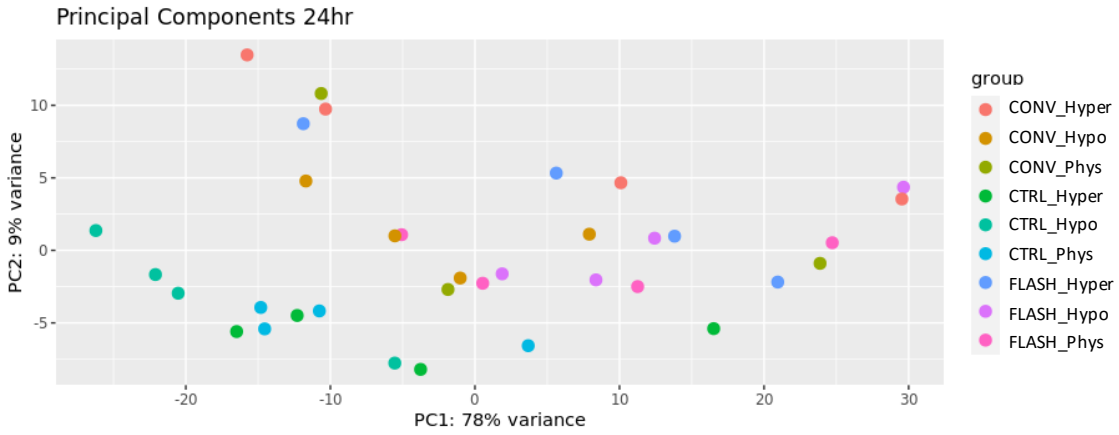

B.

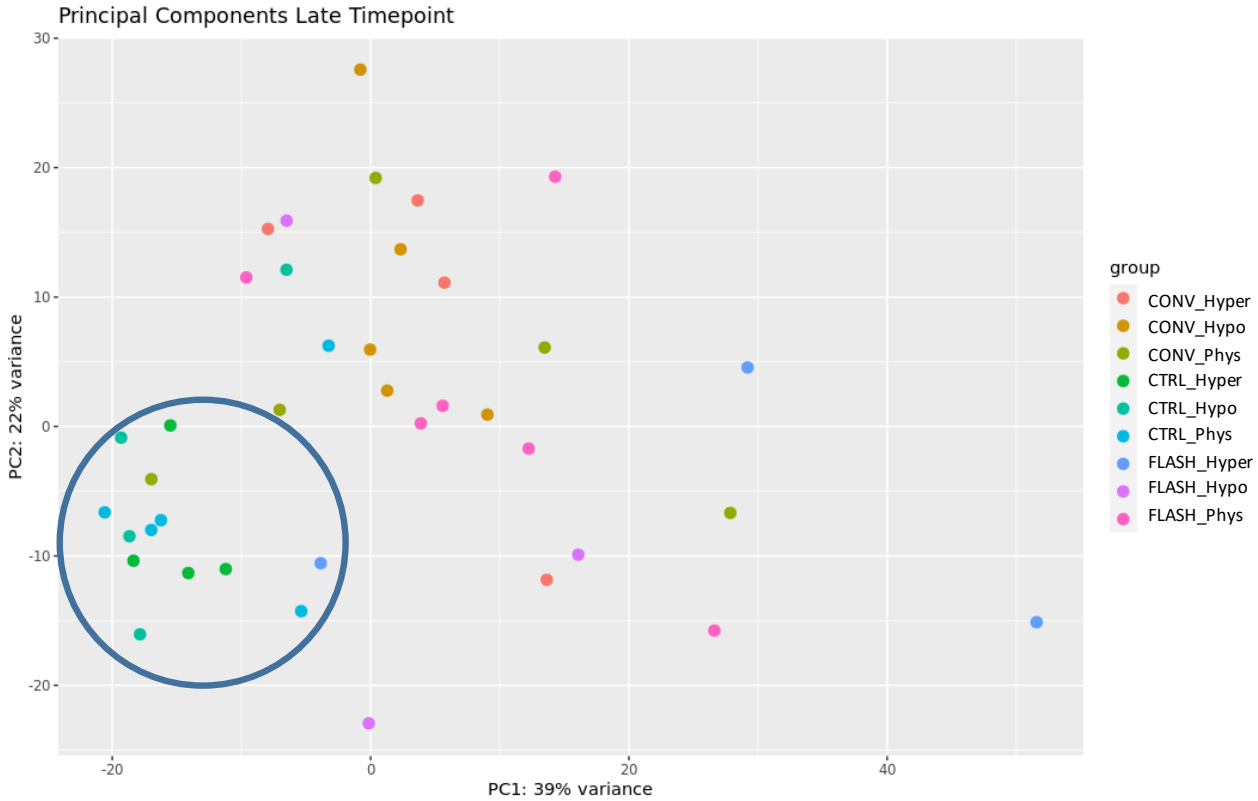

Figure 2: Data Overview

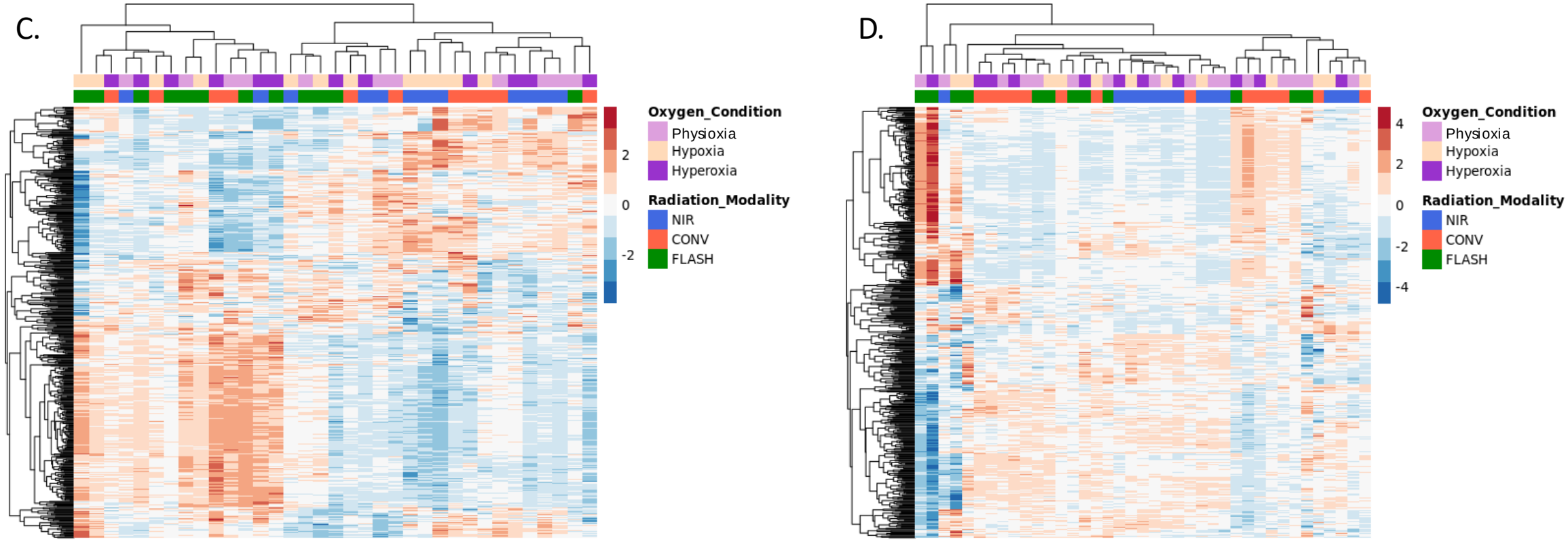

Figure 3 – Late Timepoint

A.

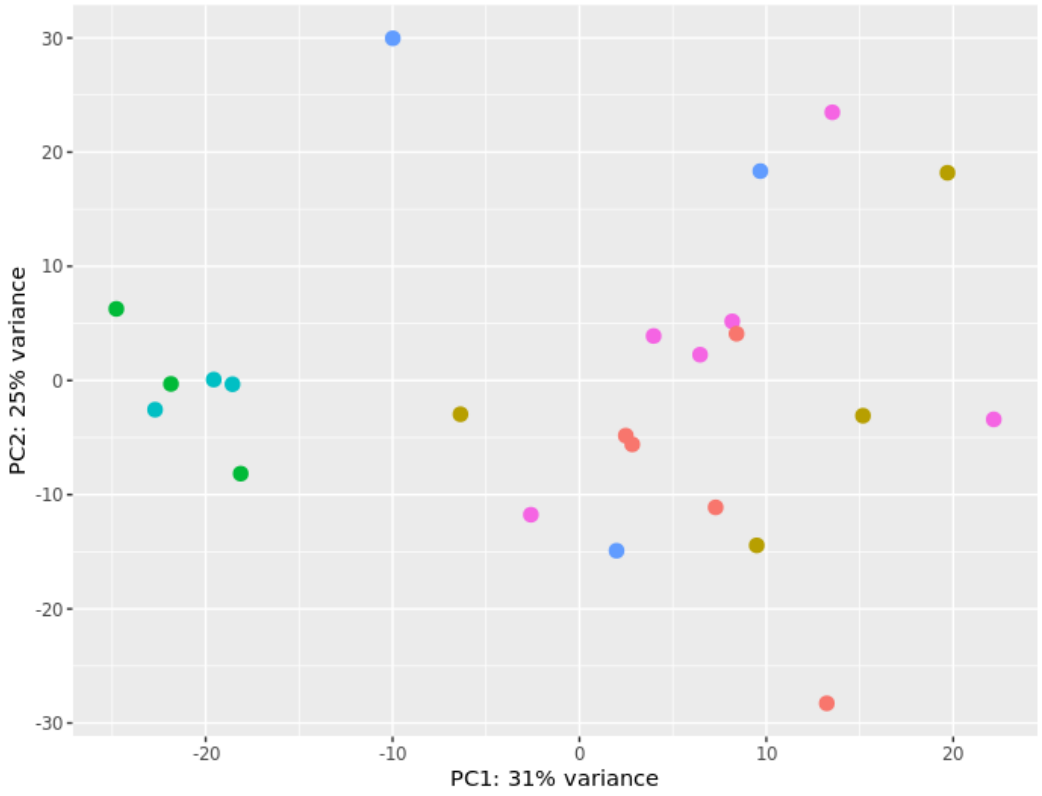

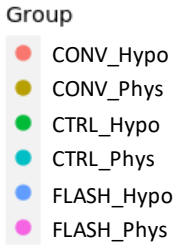

B.

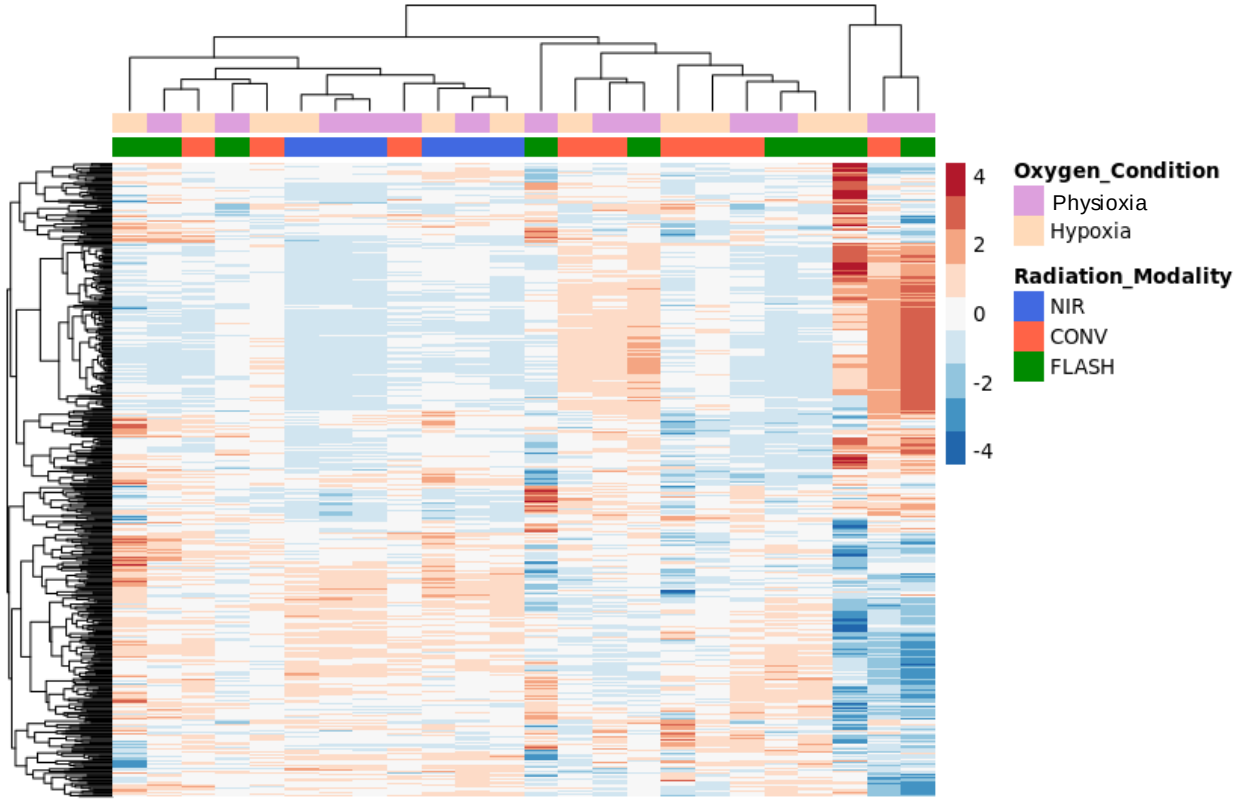

Figure 3 – Late Timepoint

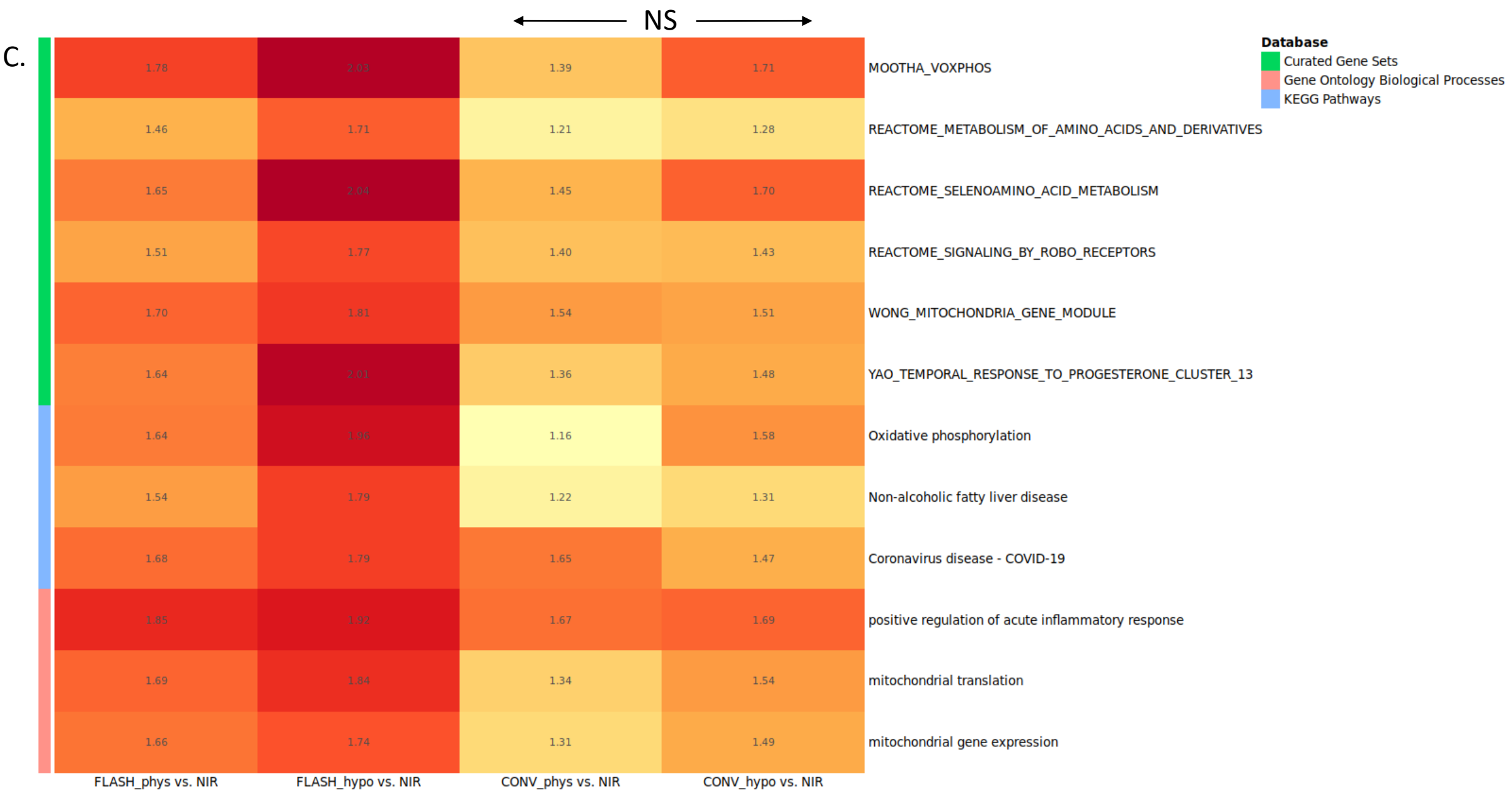

Figure 4

A.

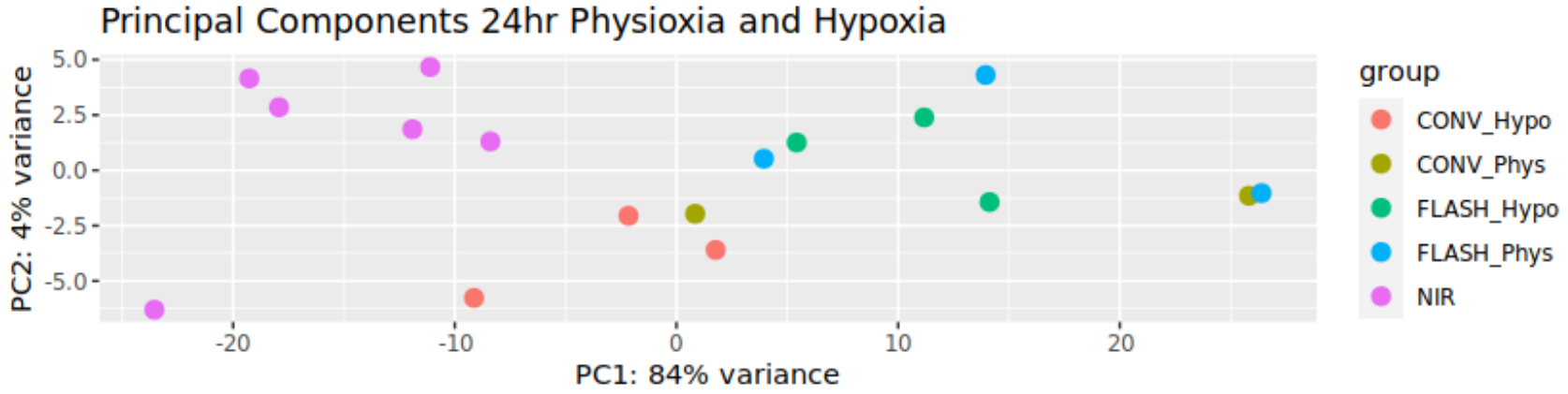
Principal Components 24hr Physioxia and Hypoxia
PC2: 4% variance
5.0
2.5
0.0
-2.5
-5.0
-20
-10
0
10
20
PC1: 84% variance
group
CONV_Hypo
CONV_Phys
FLASH_Hypo
FLASH_Phys
NIR

B.

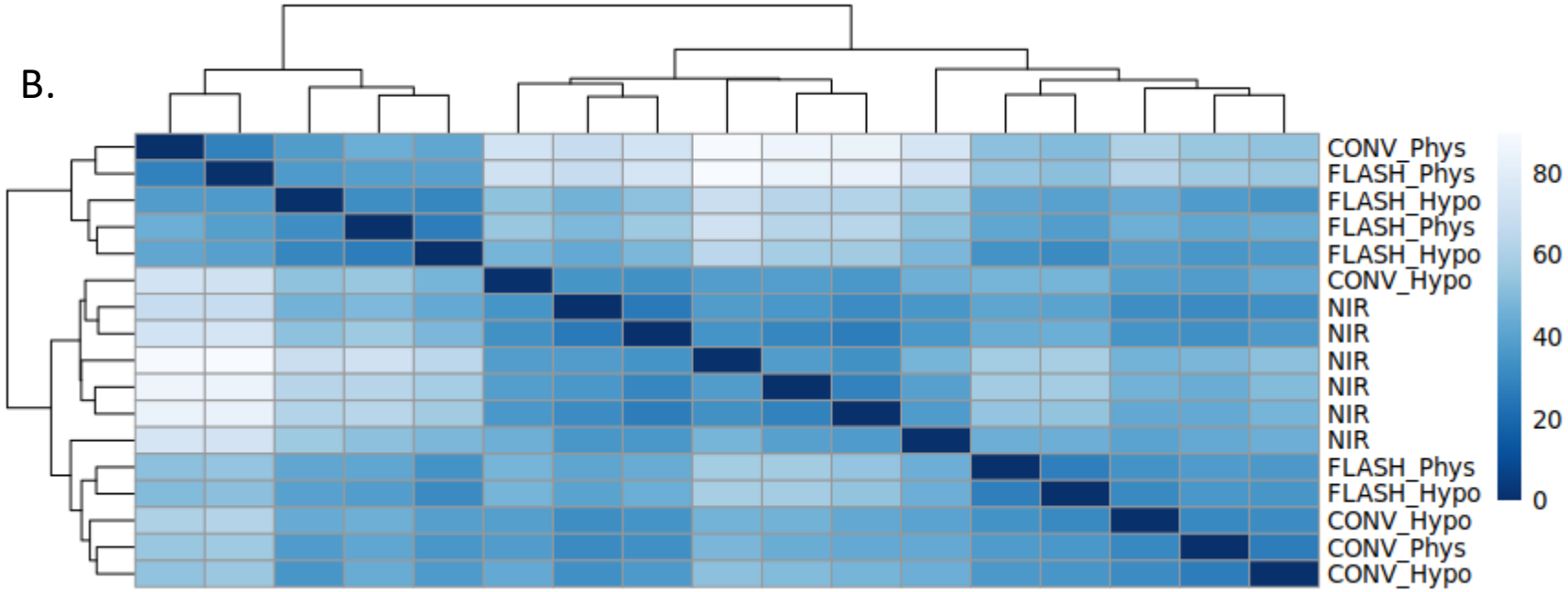
CONV_Phys
FLASH_Phys
FLASH_Hypo
FLASH_Phys
FLASH_Hypo
CONV_Hypo
NIR
NIR
NIR
NIR
NIR
NIR
FLASH_Phys
FLASH_Hypo
CONV_Hypo
CONV_Phys
CONV_Hypo
80
60
40
20
0

Figure 4 – Clamp and Normoxy – Wikipathways GSEA overlap analysis

C.

Up vs No-IR Control

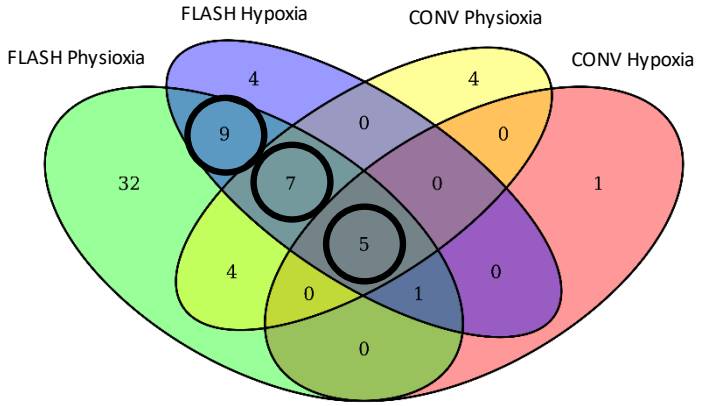

FLASH-Specific

<- NS ->

FLASH_phys vs. NIR	FLASH_hypo vs. NIR	CONV_phys vs. NIR	CONV_hypo vs. NIR	
1.89	1.76	1.63	1.58	Striated muscle contraction pathway
1.74	1.68	1.53	1.49	NRF2 pathway
1.61	1.59	1.21	1.08	Focal adhesion
1.69	1.63	1.42	1.08	Myometrial relaxation and contraction pathways
1.77	1.74	1.67	0.89	Disruption of postsynaptic signaling by CNV
1.65	1.59	1.40	1.49	Adipogenesis
1.76	1.75	1.67	1.63	Transcription factor regulation in adipogenesis
1.73	1.72	1.58	1.34	Prostaglandin and leukotriene metabolism in senescence
1.65	1.71	1.25	1.21	Complement and coagulation cascades

Tumor Delay Outcome

NS

FLASH_phys vs. NIR	FLASH_hypo vs. NIR	CONV_phys vs. NIR	CONV_hypo vs. NIR	
2.11	1.96	2.06	1.63	Inflammatory bowel disease signaling
1.96	1.90	1.76	1.73	Hematopoietic stem cell differentiation
1.90	1.79	1.64	1.43	TYROBP causal network in microglia
1.86	1.86	1.89	1.36	Glycolysis and gluconeogenesis
1.56	1.58	1.46	1.37	PI3K-Akt signaling pathway
1.81	1.76	1.77	1.29	Th17 cell differentiation pathway
1.81	1.83	1.69	1.64	Synaptic vesicle pathway

All IR

FLASH_phys vs. NIR	FLASH_hypo vs. NIR	CONV_phys vs. NIR	CONV_hypo vs. NIR	
1.85	1.79	1.63	1.56	Focal adhesion: PI3K-Akt-mTOR-signaling pathway
2.14	1.94	2.03	2.16	Overview of proinflammatory and profibrotic mediators
1.80	1.73	1.58	1.62	Nuclear receptors meta-pathway
1.88	1.84	1.72	1.65	Vitamin D receptor pathway
1.90	1.92	2.01	1.81	Development and heterogeneity of the ILC family

D.

Down vs No-IR Control

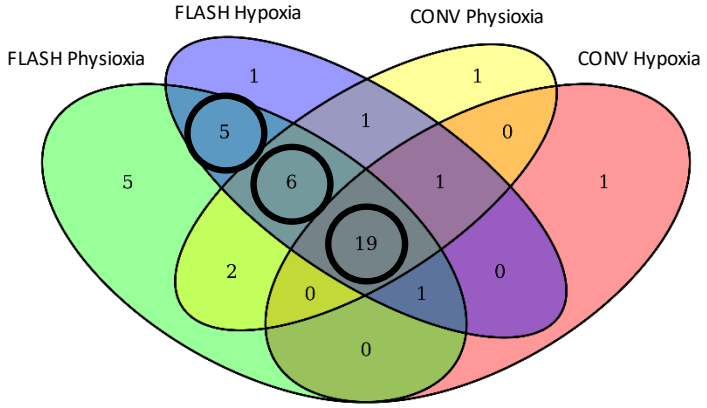

FLASH-Specific

<- NS ->

FLASH_phys vs. NIR	FLASH_hypo vs. NIR	CONV_phys vs. NIR	CONV_hypo vs. NIR	
-1.94	-1.80	-0.84	-1.19	Cytoplasmic ribosomal proteins
-1.98	-1.77	-1.55	-1.46	Eukaryotic transcription initiation
-1.98	-1.95	-1.85	-1.09	Mitochondrial complex III assembly
-1.56	-1.61	-1.33	-1.41	Genes related to primary cilium development
-1.76	-1.89	-1.56	-1.53	Purine metabolism and related disorders

Tumor Delay Outcome

NS

FLASH_phys vs. NIR	FLASH_hypo vs. NIR	CONV_phys vs. NIR	CONV_hypo vs. NIR	
-2.88	-2.77	-2.52	0.73	Electron transport chain: OXPHOS system in mitochondria
-2.58	-2.45	-2.08	0.83	Oxidative phosphorylation
-2.52	-2.40	-2.29	0.70	Mitochondrial complex I assembly model OXPHOS system
-2.28	-2.09	-1.93	0.86	Mitochondrial complex IV assembly
-1.88	-1.60	-1.60	-1.44	miRNA regulation of DNA damage response
-1.93	-1.84	-1.78	-1.70	Nucleotide excision repair

All IR

FLASH_phys vs. NIR	FLASH_hypo vs. NIR	CONV_phys vs. NIR	CONV_hypo vs. NIR	
-2.97	-2.90	-2.99	-3.05	Retinoblastoma gene in cancer
-2.69	-2.56	-2.61	-2.58	Cell cycle
-2.76	-2.85	-2.87	-2.92	DNA replication
-2.65	-2.62	-2.50	-2.50	DNA IR-damage and cellular response via ATR
-2.47	-2.38	-2.41	-2.41	DNA repair pathways, full network
-2.41	-2.35	-2.41	-2.42	G1 to S cell cycle control
-2.20	-2.12	-2.09	-1.95	Pyrimidine metabolism
-2.20	-2.08	-2.02	-2.14	DNA IR-double strand breaks and cellular response via ATM
-2.28	-2.42	-2.41	-2.35	Gastric cancer network 1
-2.25	-2.10	-2.15	-2.21	DNA mismatch repair

Figure 4 – Clamp and Normoxy – Regulatory GSEA overlap analysis

E. Up vs No-IR Control

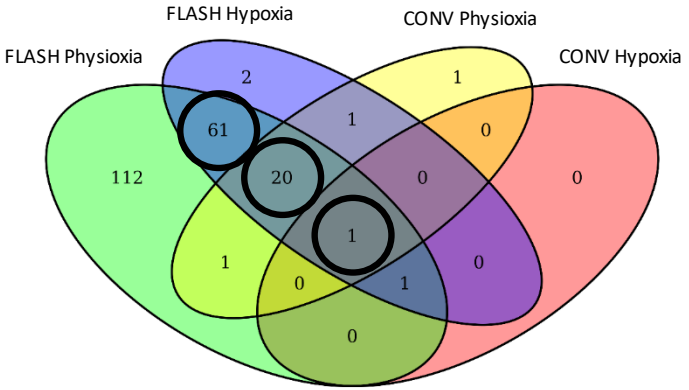

FLASH-Specific

<- NS ->

1.93	1.70	1.42	1.06	MIR149_3P
1.89	1.68	1.37	1.01	MIR6883_5P
1.85	1.75	1.47	1.46	GATAAGR_GATA_C
1.74	1.64	1.33	1.36	MIR6825_5P
1.75	1.63	1.50	1.33	NFXL1_TARGET_GENES
1.75	1.73	1.36	1.13	MIR6721_5P
1.83	1.64	1.52	1.29	NFKB_Q6
1.84	1.75	1.51	1.17	MIR6756_5P
1.81	1.73	1.45	1.42	MYOGENIN_Q6
1.85	1.70	1.53	1.22	LBP1_Q6
FLASH_phys vs. NIR	FLASH_hypo vs. NIR	CONV_phys vs. NIR	CONV_hypo vs. NIR	

Tumor Delay Outcome

NS

1.90	1.87	1.55	1.47	ZNF436_TARGET_GENES
1.98	1.93	1.82	1.43	NFKAPPAB_01
1.79	1.71	1.54	1.28	TGGNNNNNNKCCAR_UNKNOWN
1.89	1.70	1.75	1.29	NFKB_C
1.88	1.67	1.68	1.38	HEB_Q6
1.79	1.61	1.58	1.42	CCCNNGGGAR_OLF1_01
1.82	1.64	1.61	1.54	E12_Q6
1.85	1.71	1.68	1.33	SMAD3_Q6
1.82	1.75	1.76	1.40	NFKB_Q6_01
1.77	1.61	1.69	1.39	BACH2_01
1.75	1.63	1.65	1.26	CP2_01
1.75	1.64	1.56	1.23	CREL_01
1.71	1.61	1.58	1.20	IK1_01
1.72	1.72	1.69	1.58	MYOD_Q6
1.71	1.54	1.64	1.34	HIF1_Q5
1.72	1.68	1.63	1.51	HNF1_Q6
1.76	1.73	1.82	1.29	CAGNWMCNNNGAC_UNKNOWN
FLASH_phys vs. NIR	FLASH_hypo vs. NIR	CONV_phys vs. NIR	CONV_hypo vs. NIR	

All IR

2.14	1.99	1.82	1.78	CCANNAGRKGGC_UNKNOWN
FLASH_phys vs. NIR	FLASH_hypo vs. NIR	CONV_phys vs. NIR	CONV_hypo vs. NIR	

F. Down vs No-IR Control

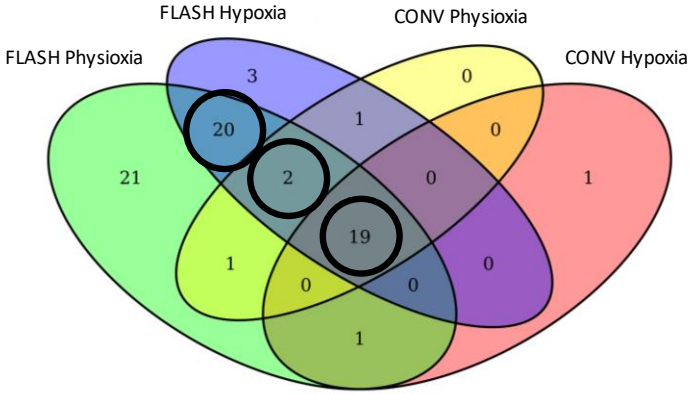

FLASH-Specific

<- NS ->

-1.76	-1.57	-1.37	-1.16	RORA_TARGET_GENES
-1.61	-1.51	-1.34	-1.28	CIC_TARGET_GENES
-1.85	-1.69	-1.24	-1.33	CHAMP1_TARGET_GENES
-1.88	-1.60	-1.30	-1.08	MXD1_TARGET_GENES
-1.66	-1.51	-1.15	-1.23	EMX1_TARGET_GENES
-1.71	-1.60	-1.45	-0.65	SETBP1_TARGET_GENES
-1.52	-1.47	-1.17	-0.82	CASP8AP2_TARGET_GENES
-1.45	-1.38	-1.16	-1.18	SRPK1_TARGET_GENES
-1.59	-1.47	-0.90	-1.17	MIR372_5P
-1.59	-1.44	-1.18	-1.18	MYBL1_TARGET_GENES
FLASH_phys vs. NIR	FLASH_hypo vs. NIR	CONV_phys vs. NIR	CONV_hypo vs. NIR	

All IR

-2.29	-2.35	-2.28	-2.44	E2F1_Q6
-2.22	-2.27	-2.27	-2.39	E2F_02
-2.21	-2.27	-2.28	-2.34	E2F_Q6
-2.23	-2.28	-2.28	-2.39	E2F1DP1_01
-2.23	-2.28	-2.28	-2.39	E2F1DP2_01
-2.21	-2.25	-2.18	-2.31	E2F4DP1_01
-2.23	-2.28	-2.28	-2.39	E2F4DP2_01
-2.40	-2.41	-2.42	-2.48	SGCGSSAAA_E2F1DP2_01
-2.24	-2.27	-2.31	-2.35	E2F_Q4
-2.09	-2.13	-2.05	-2.23	E2F1_Q3
FLASH_phys vs. NIR	FLASH_hypo vs. NIR	CONV_phys vs. NIR	CONV_hypo vs. NIR	

Tumor Delay Outcome

NS

-1.91	-1.80	-1.81	-1.16	FOXR2_TARGET_GENES
-1.88	-1.84	-2.03	-1.17	ZNF704_TARGET_GENES
FLASH_phys vs. NIR	FLASH_hypo vs. NIR	CONV_phys vs. NIR	CONV_hypo vs. NIR	

Figure 5

A.

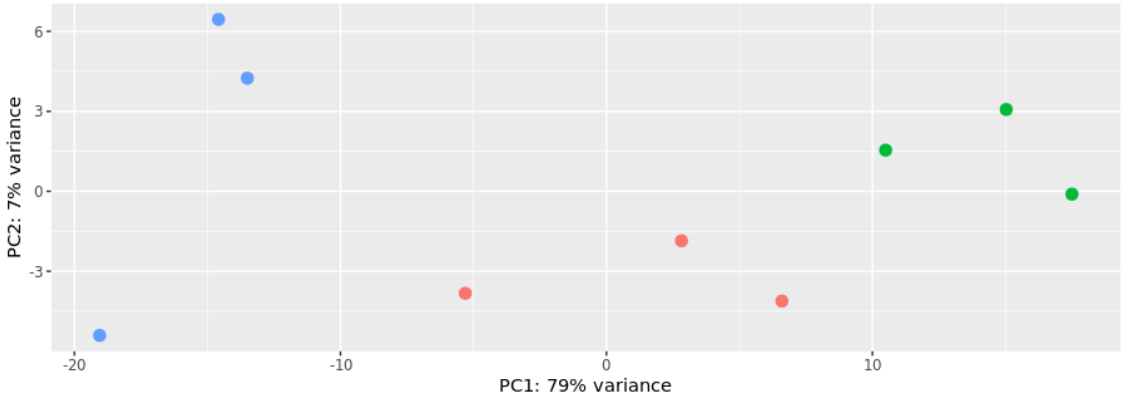
6
3
0
-3
PC2: 7% variance
-20
-10
0
10
PC1: 79% variance
group
CONV
FLASH
NIR

B.

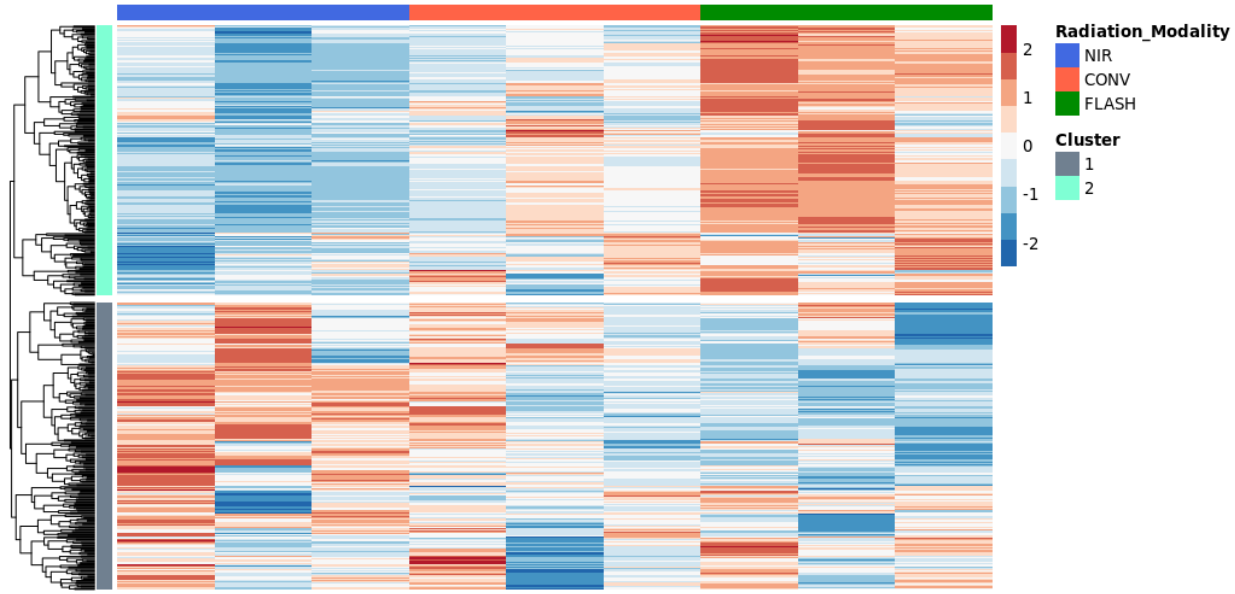
2
1
0
-1
-2
Radiation_Modality
NIR
CONV
FLASH
Cluster
1
2

Figure 5

C. Cluster 1 Enrichments – Down in FLASH

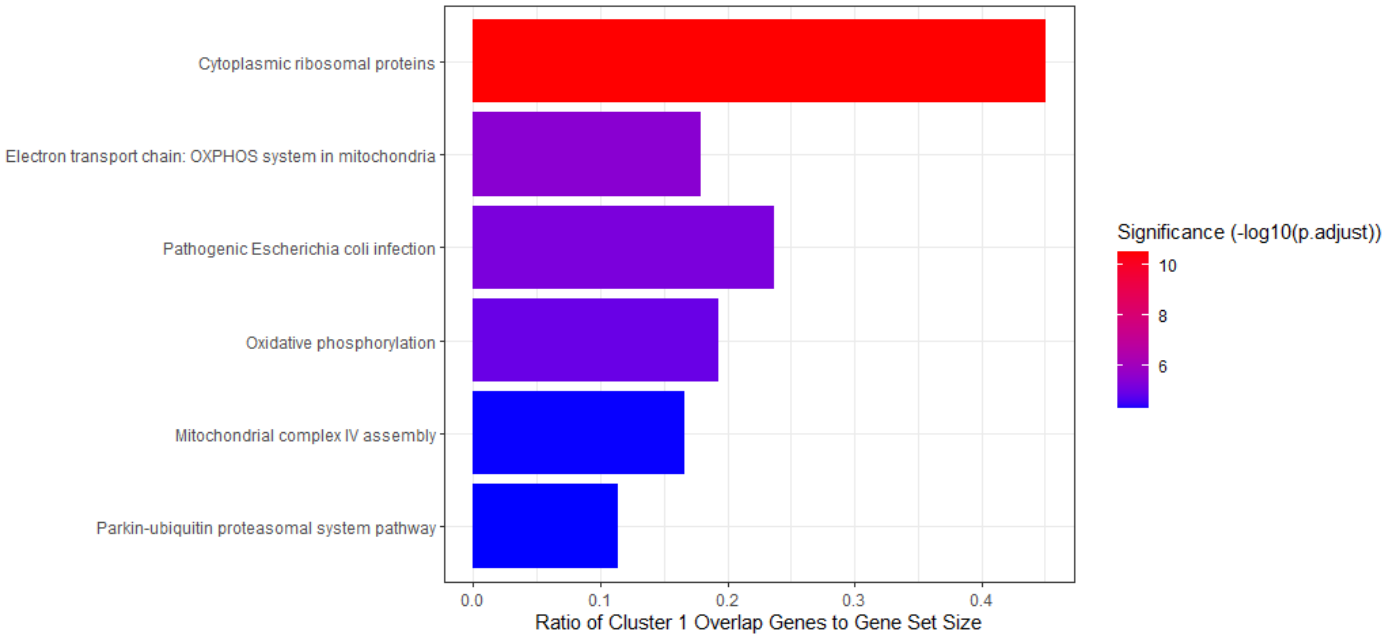

D. Cluster 2 Enrichments – Up in FLASH

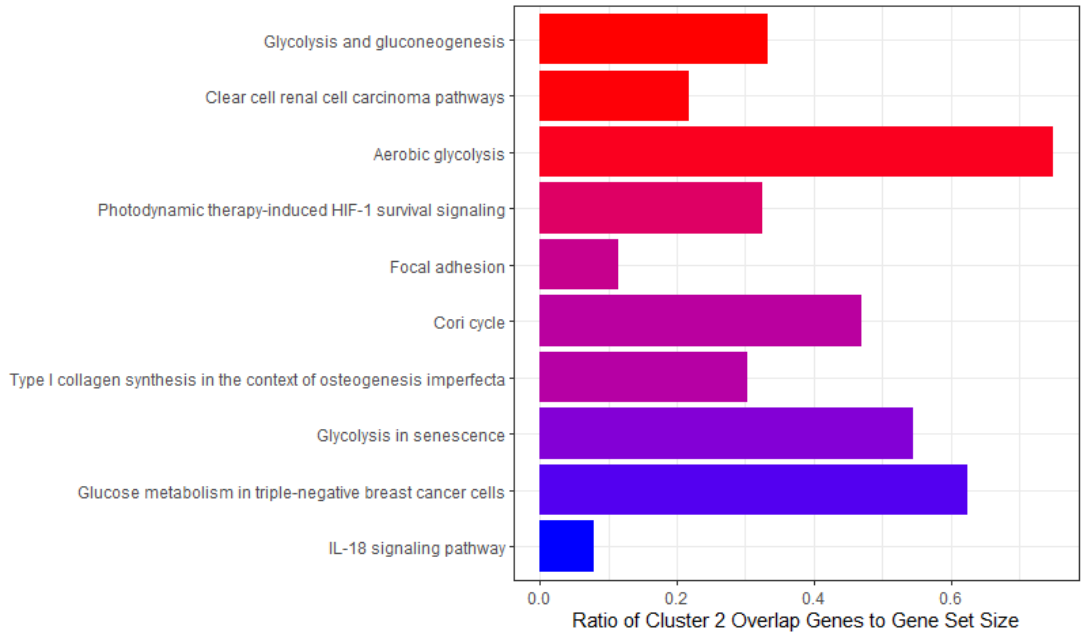

E.

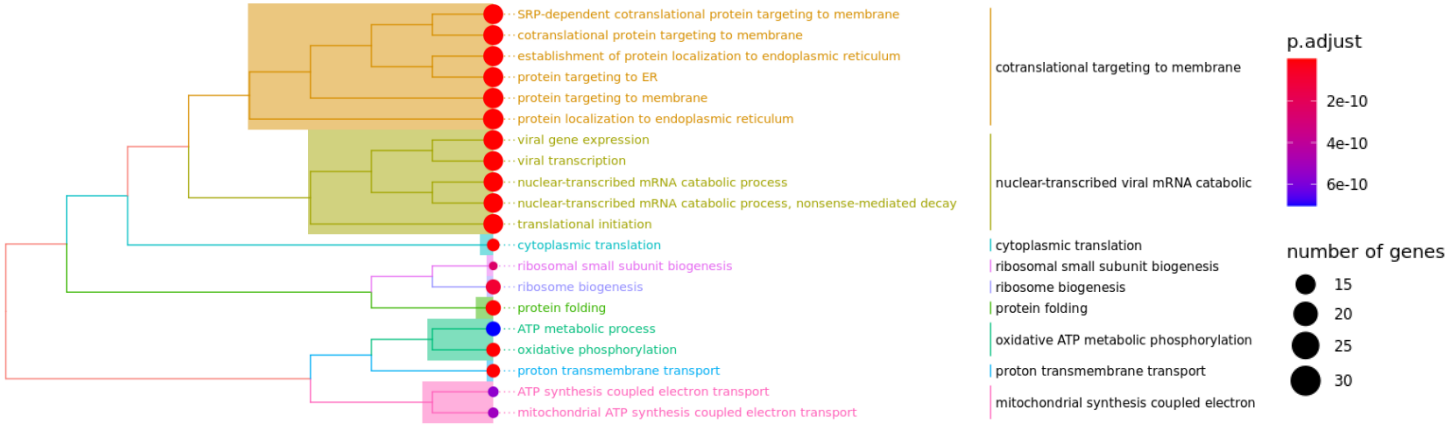

F.

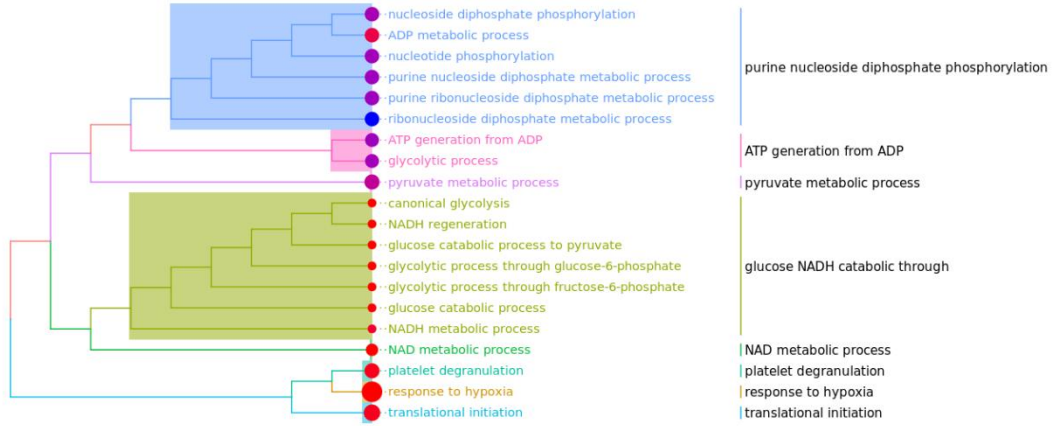

Figure 6 – GSEA Enrichment Plots Clamp

A.

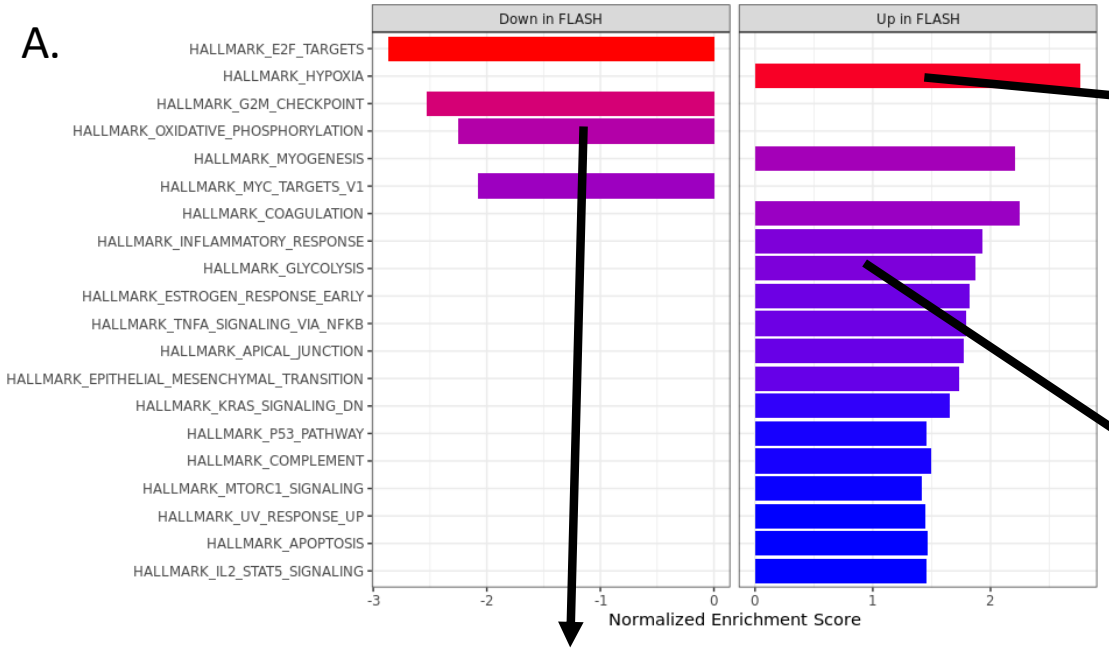

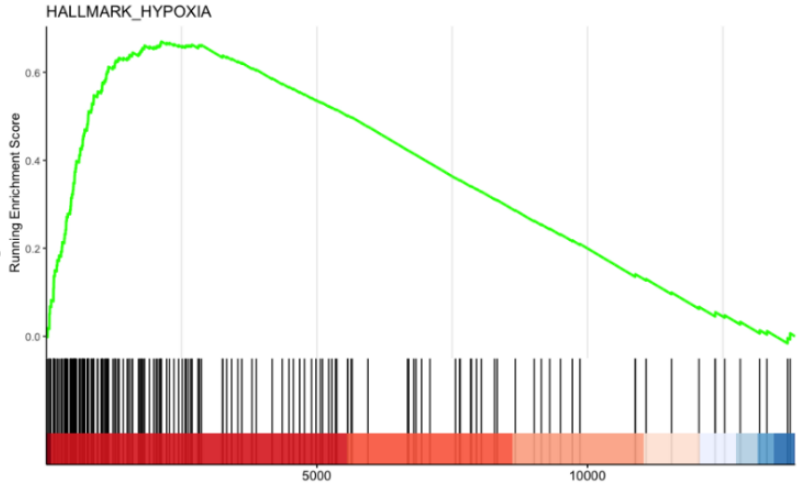

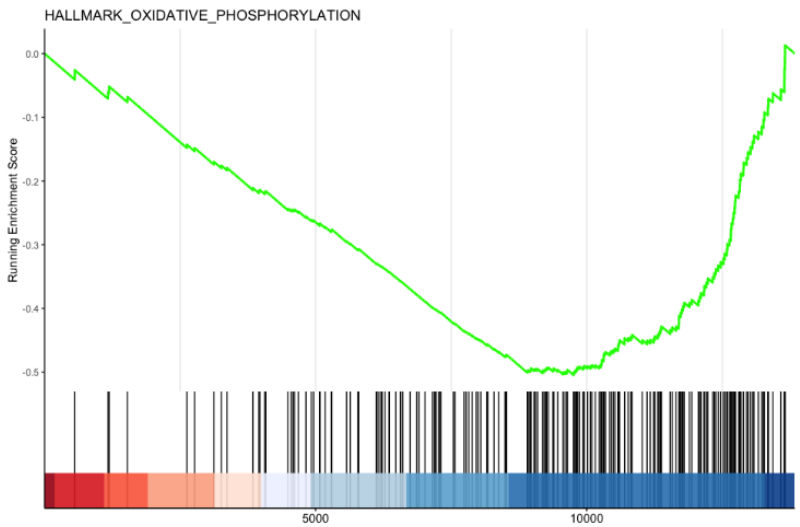

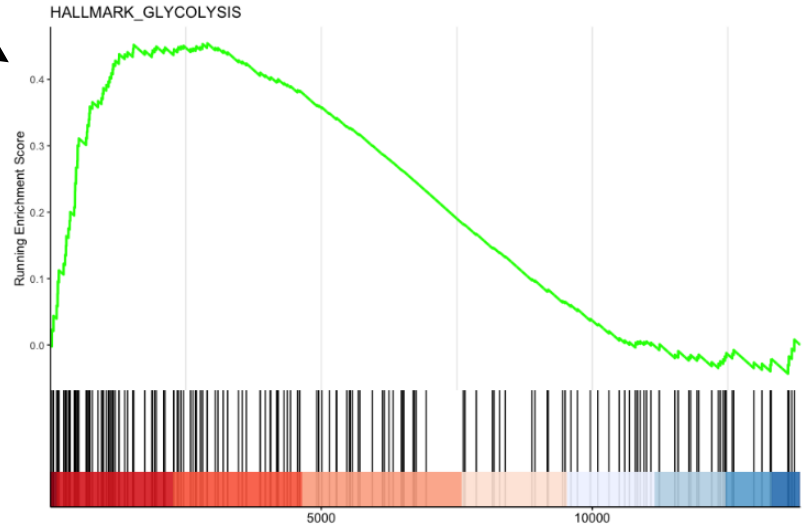

Fig6 – Metabolic Pathways

B.

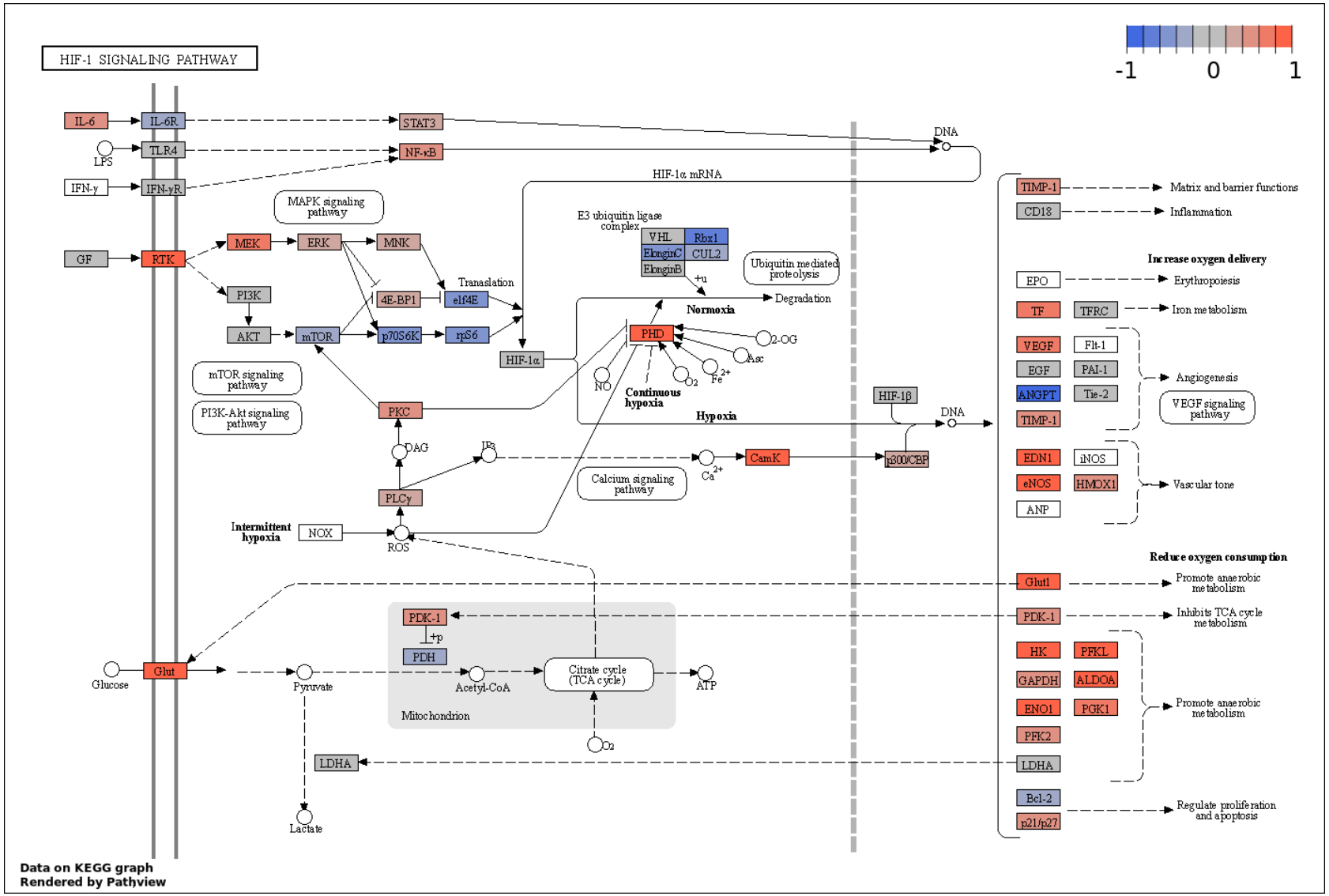

Fig6 – Metabolic Pathways

C.

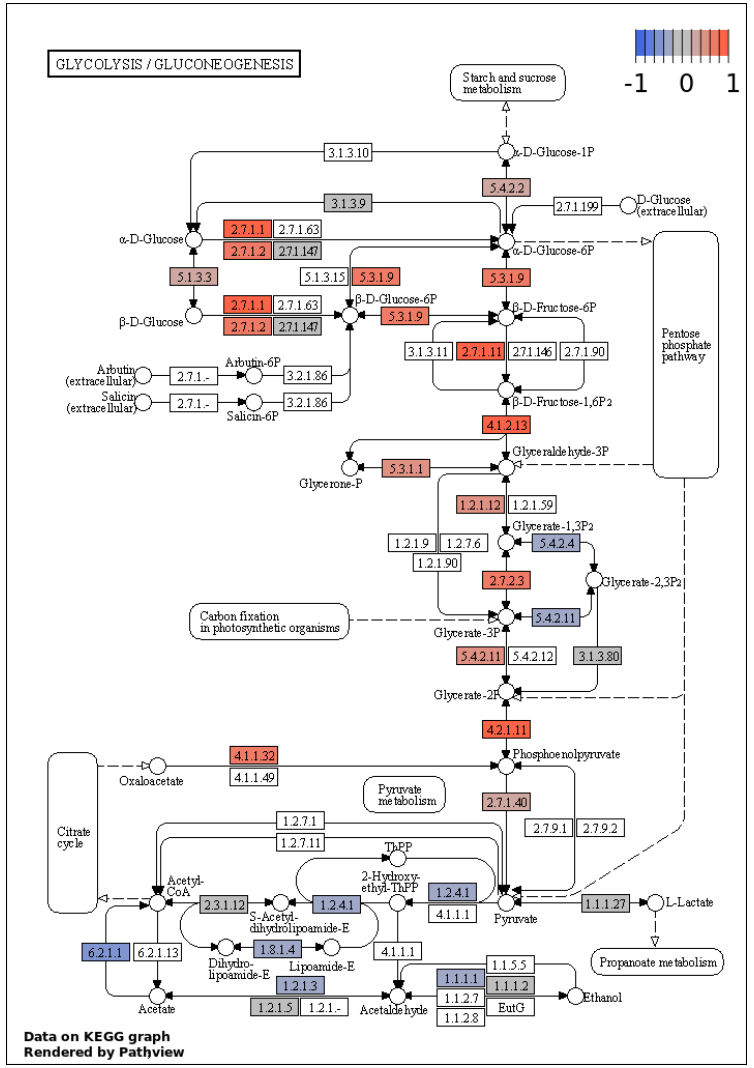

D.

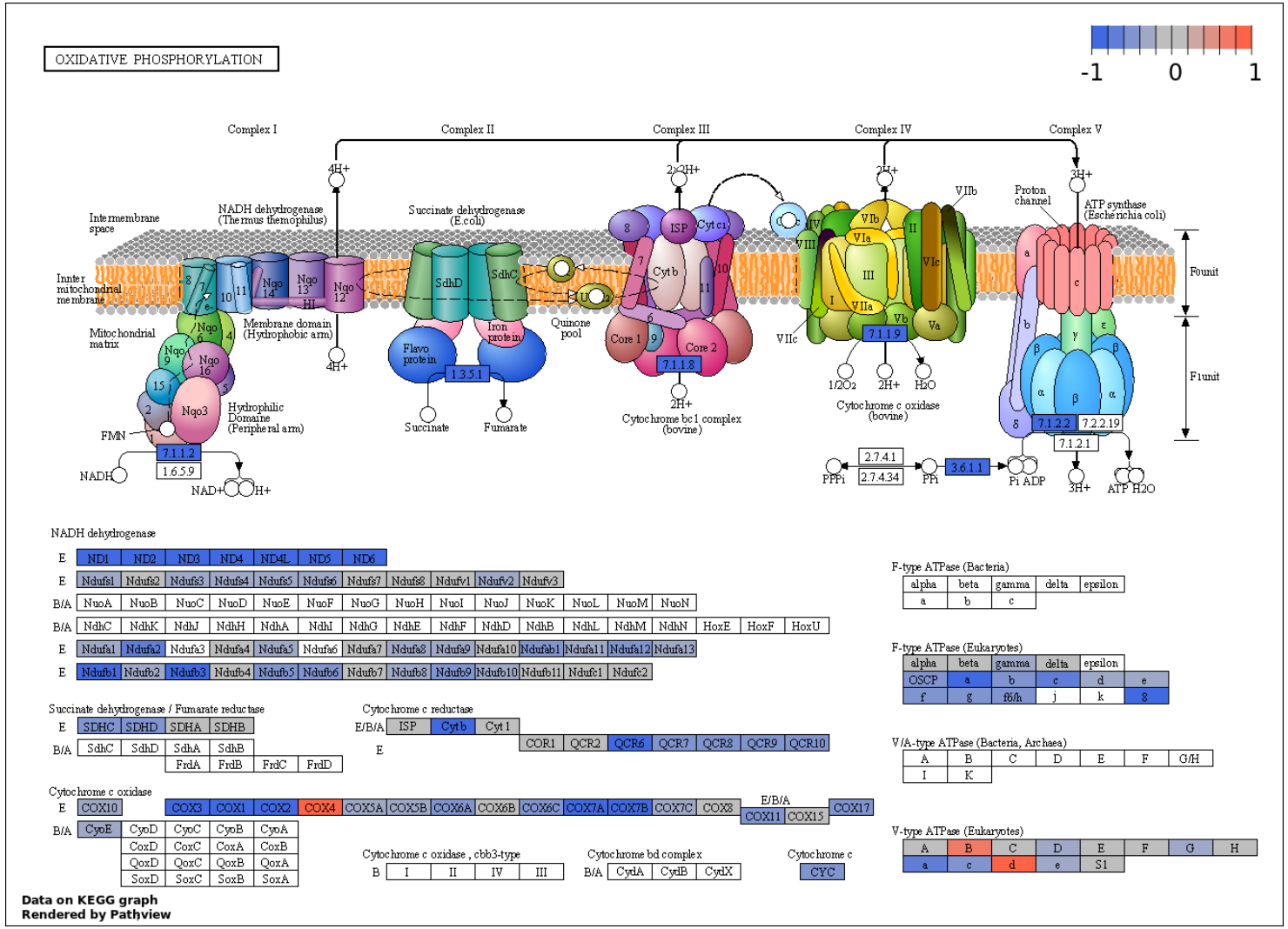

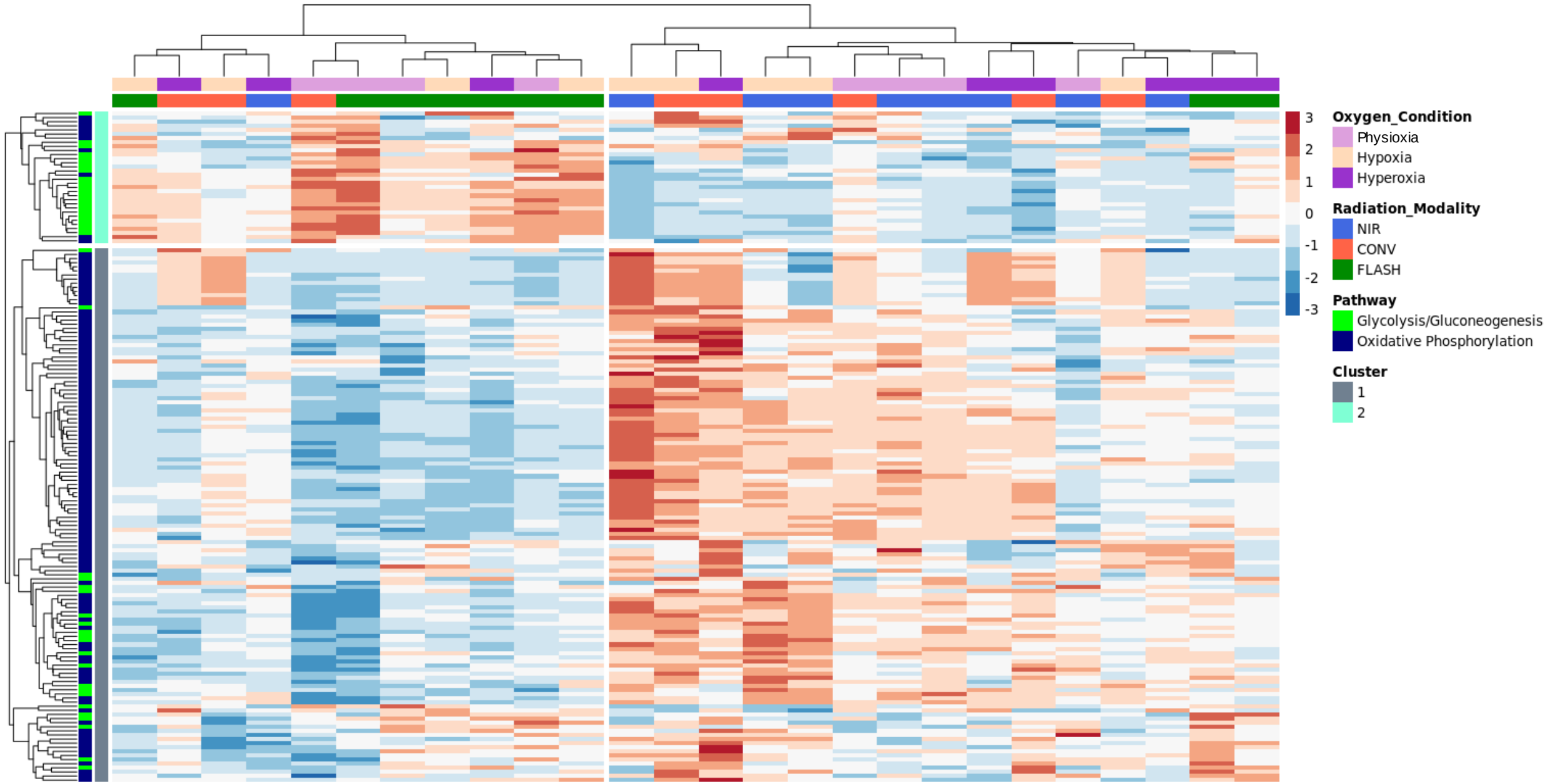
3
2
1
0
-1
-2
-3
Oxygen_Condition
Physioxia
Hypoxia
Hyperoxia
Radiation_Modality
NIR
CONV
FLASH
Pathway
Glycolysis/Gluconeogenesis
Oxidative Phosphorylation
Cluster
1
2

Supplementary Figures

S1 – U-87 MG GBM Independent Experiment

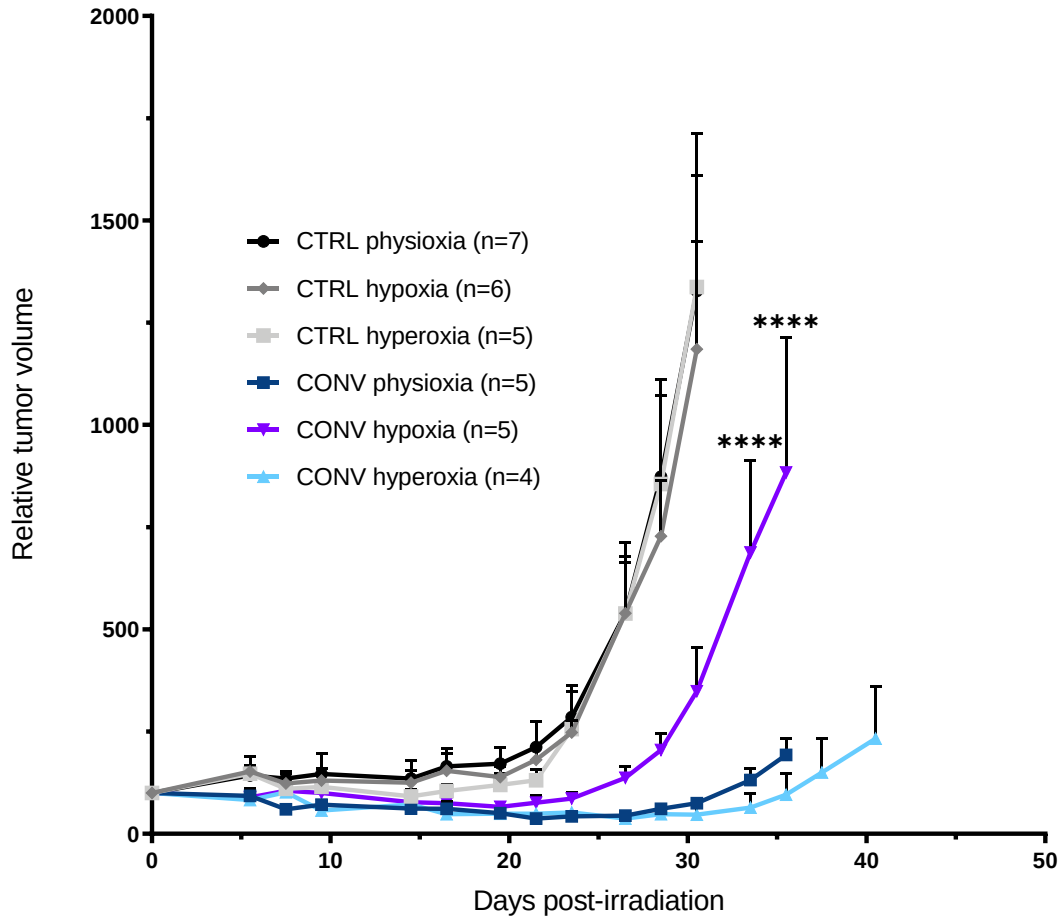

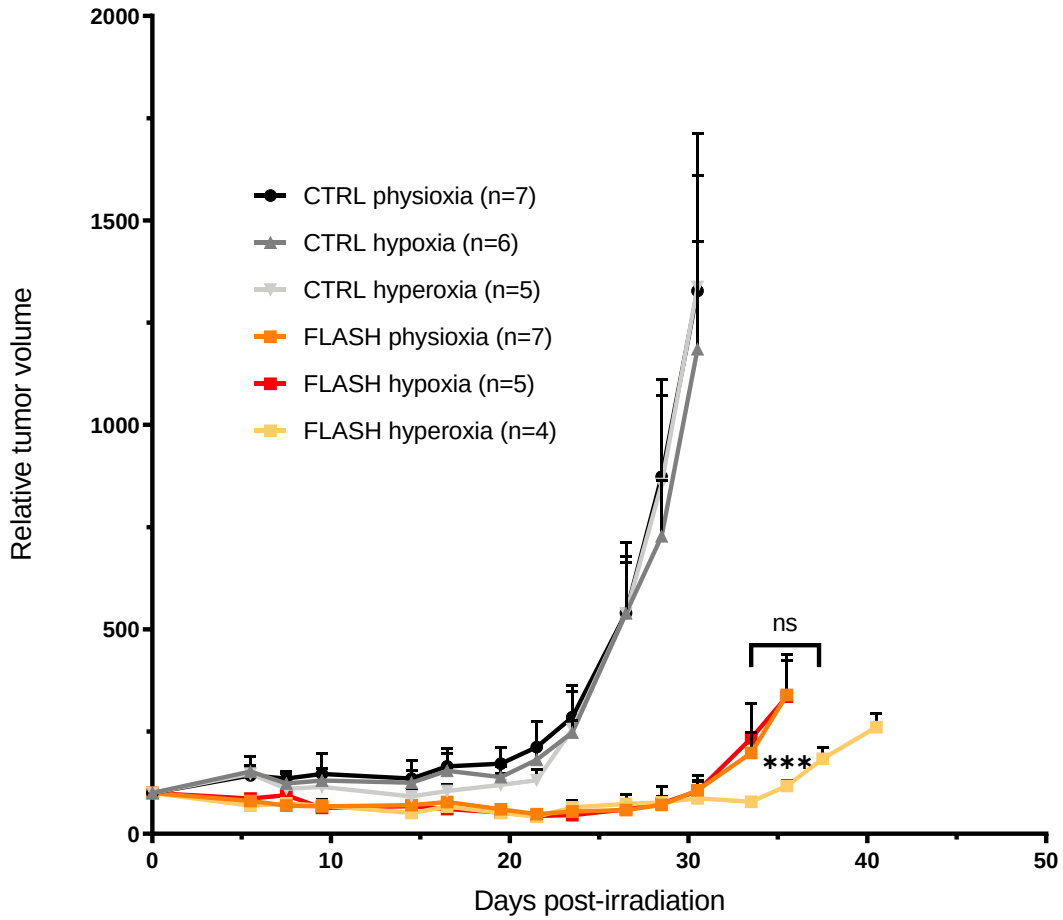

S2 – H454 Mouse GBM

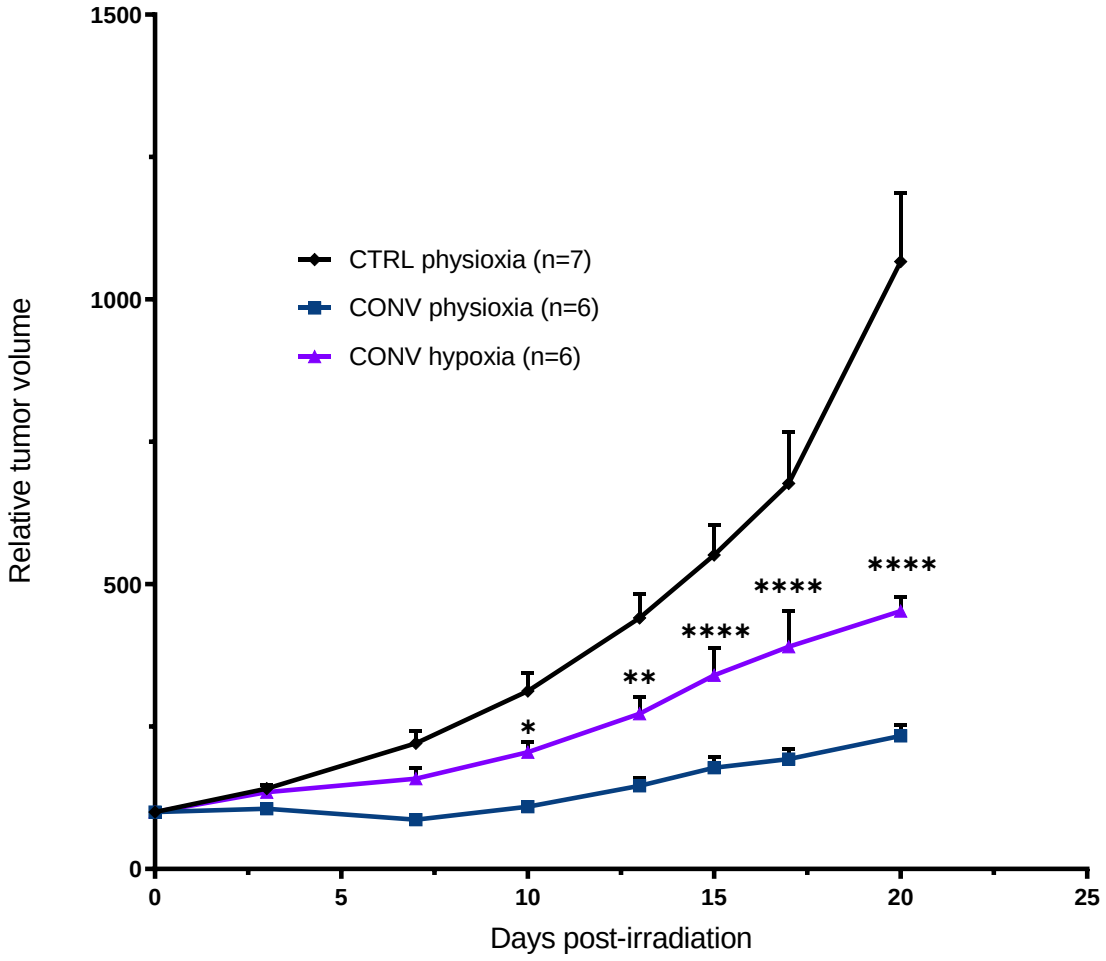

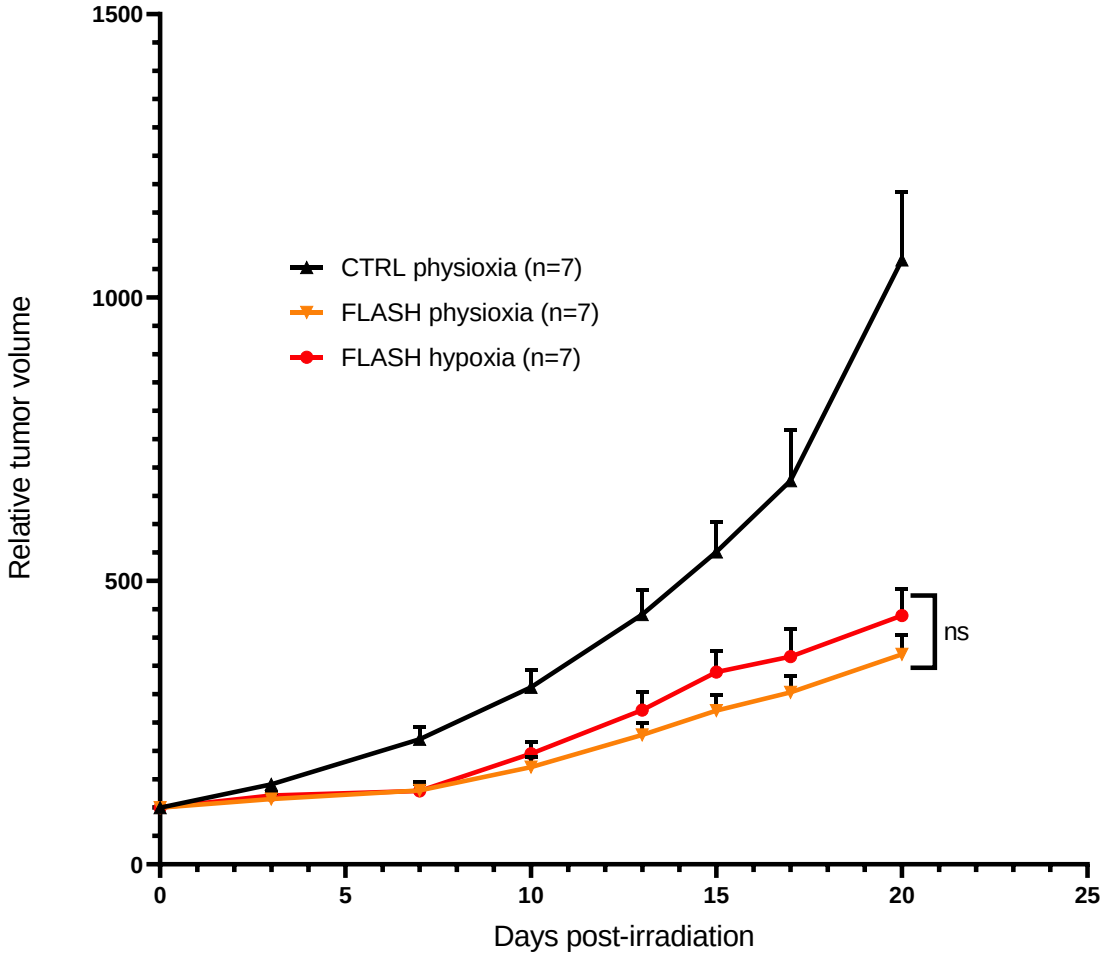

S3

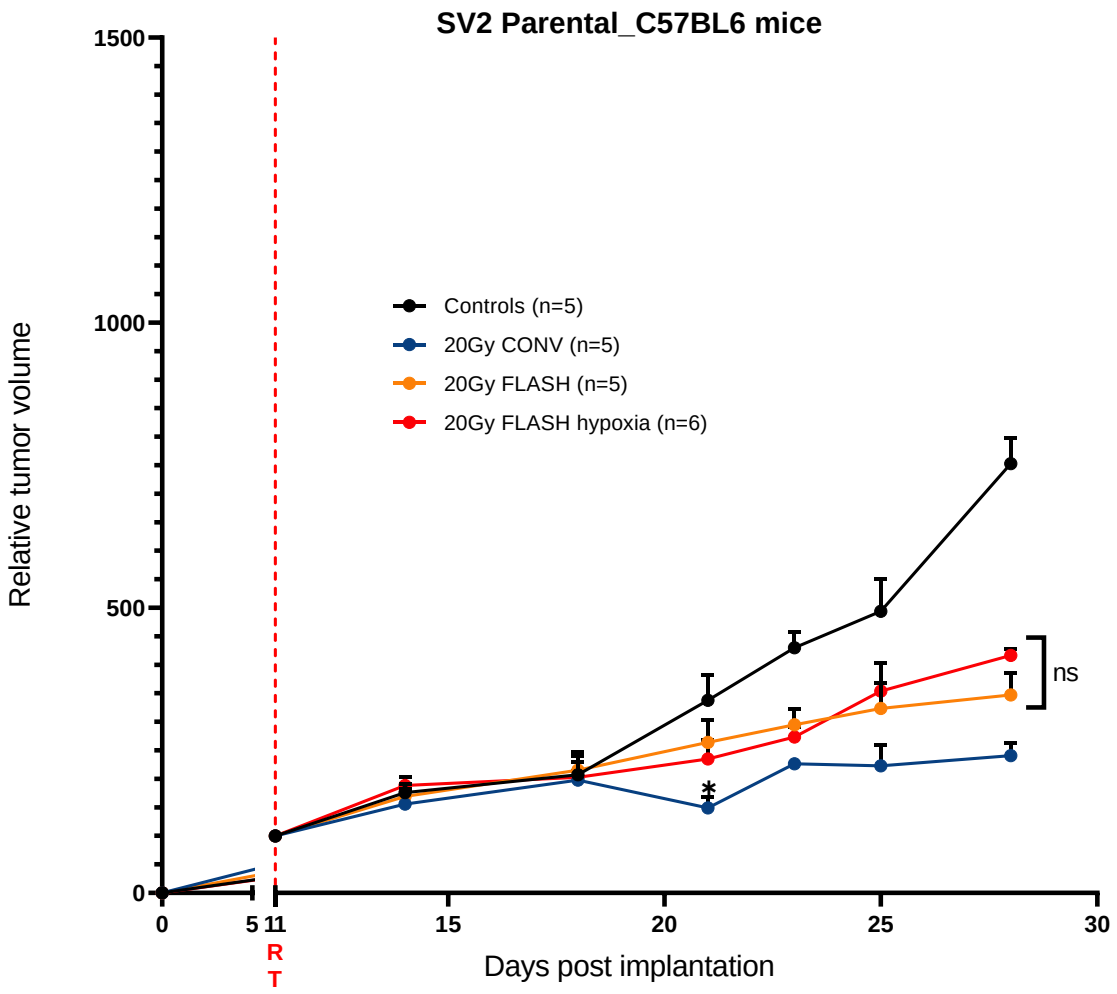
SV2 Parental_C57BL6 mice
Relative tumor volume
1500
1000
500
0
Controls (n=5)
20Gy CONV (n=5)
20Gy FLASH (n=5)
20Gy FLASH hypoxia (n=6)
ns
*
0
5
11
15
20
25
30
RT
Days post implantation

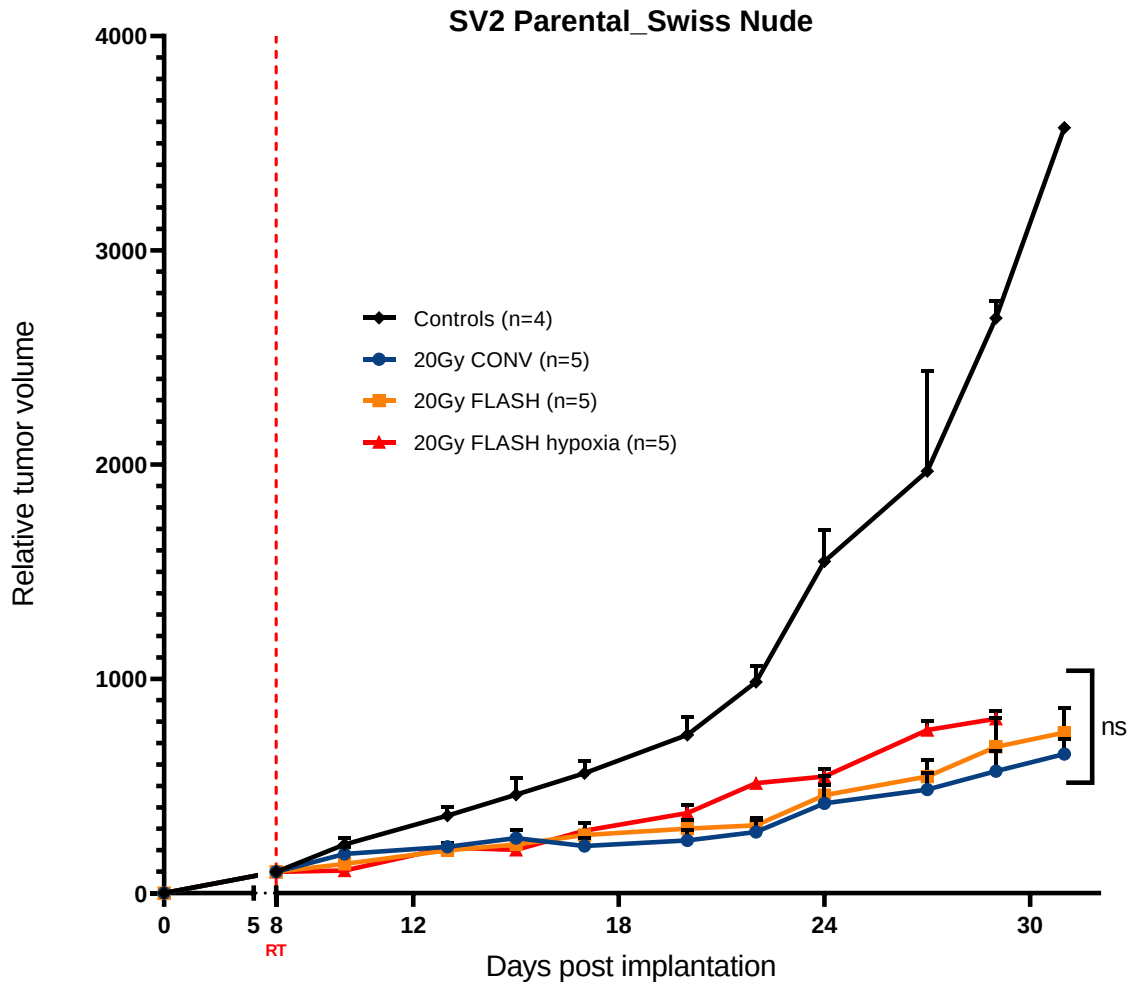
SV2 Parental_Swiss Nude
Relative tumor volume
4000
3000
2000
1000
0
Controls (n=4)
20Gy CONV (n=5)
20Gy FLASH (n=5)
20Gy FLASH hypoxia (n=5)
ns
0
5
8
12
18
24
30
RT
Days post implantation

S4

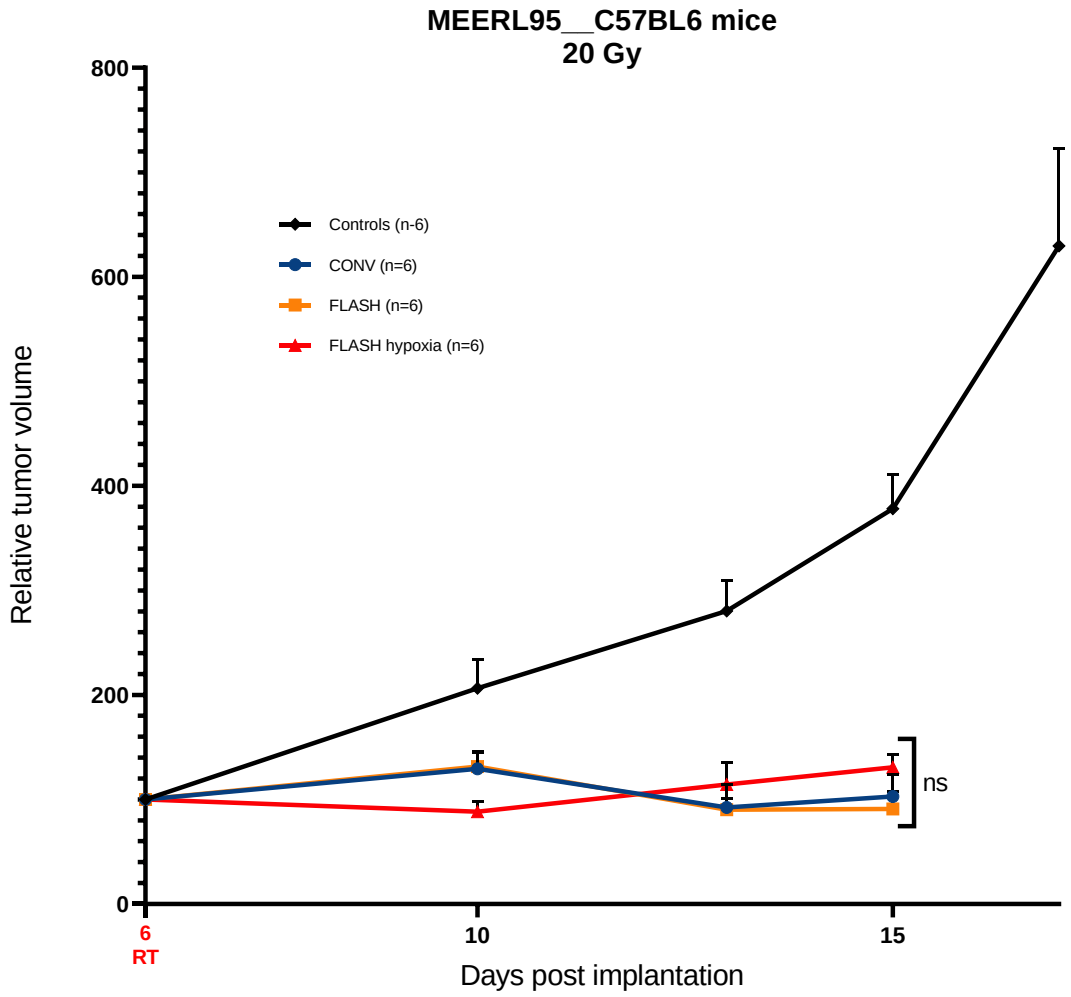
MEERL95__C57BL6 mice
20 Gy
Relative tumor volume
800
600
400
200
0
Controls (n-6)
CONV (n=6)
FLASH (n=6)
FLASH hypoxia (n=6)
ns
6
RT
10
15
Days post implantation

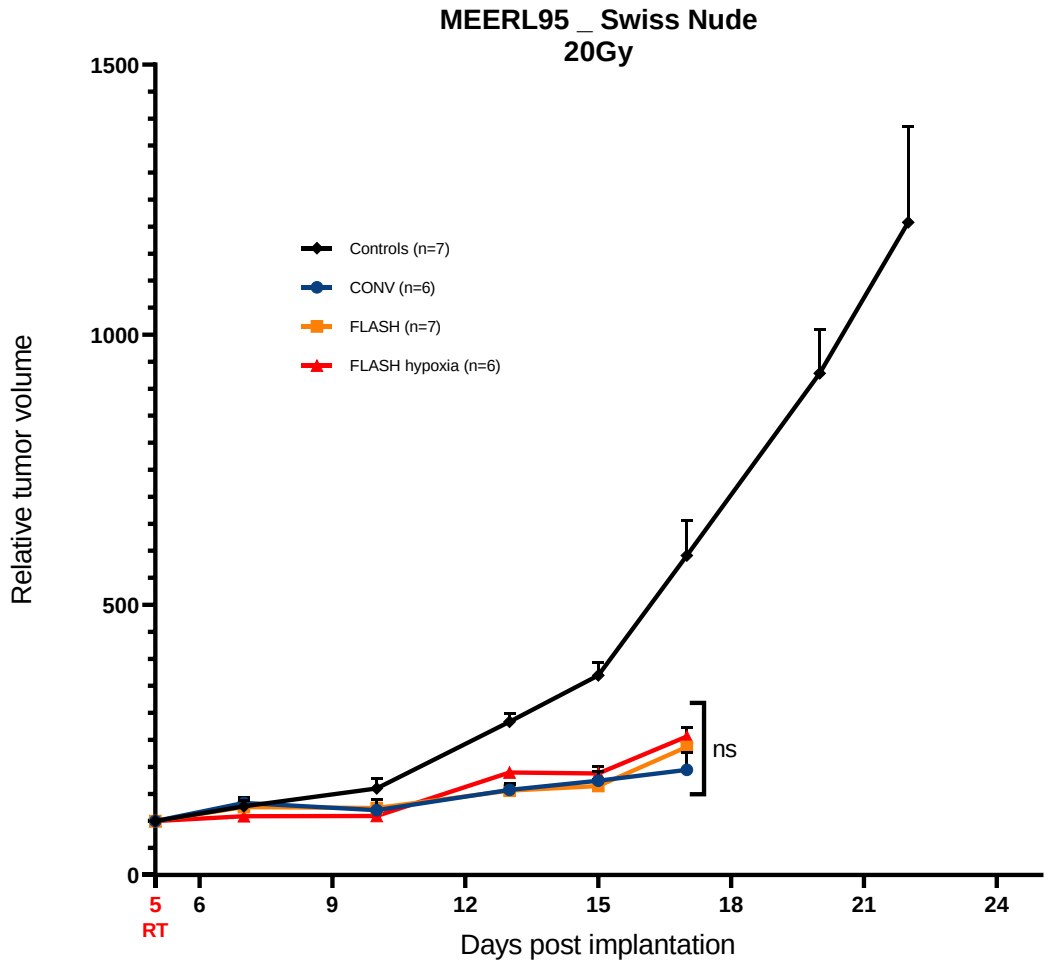
MEERL95 _ Swiss Nude
20Gy
Relative tumor volume
1500
1000
500
0
Controls (n=7)
CONV (n=6)
FLASH (n=7)
FLASH hypoxia (n=6)
ns
5
RT
6
9
12
15
18
21
24
Days post implantation

Figure S5: Pimonidazole Staining

Hypoxia (Clamp)

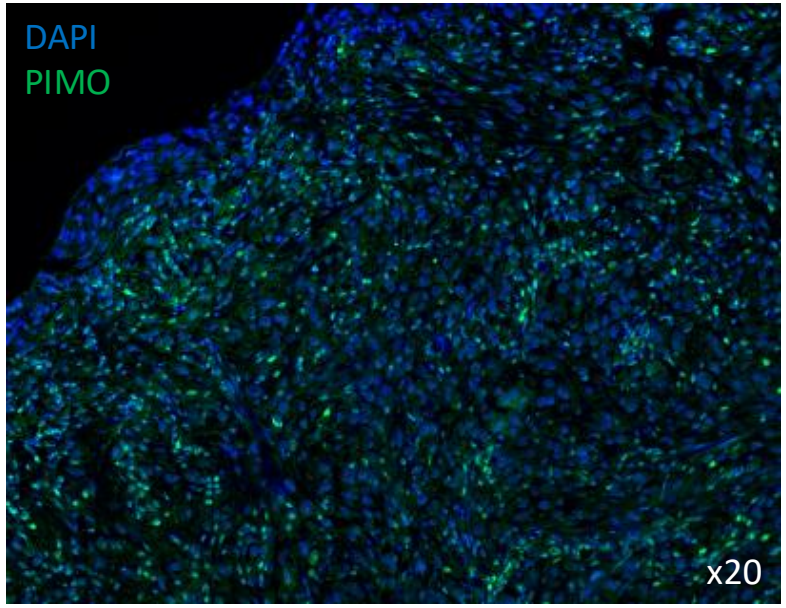

Physioxia

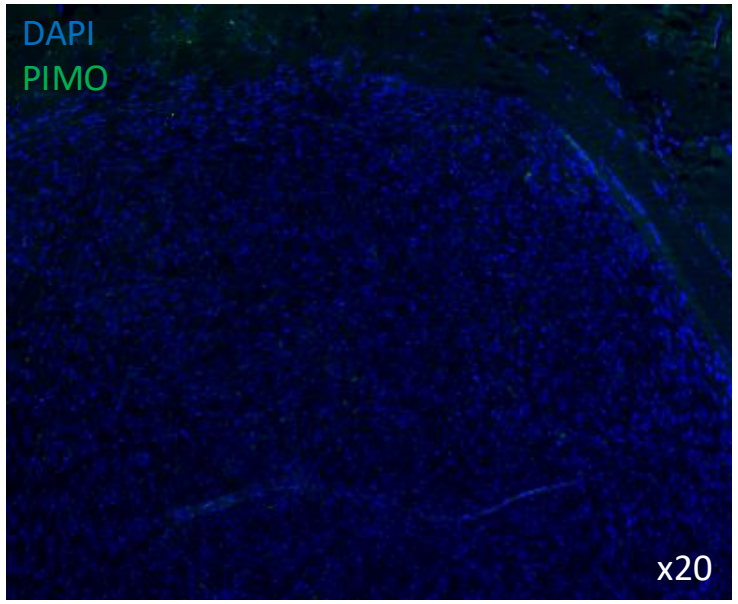

Hyperoxia (Carbogen)